Available online at www.sciencedirect.com
ScienceDirect
Journal of Sound and Vibration 321 (2009) 735–761
JOURNAL OF SOUND AND VIBRATION
www.elsevier.com/locate/jsvi

Stochastic response analysis of piezoelectric axisymmetric hollow cylinders

Z.G. Ying[a,*], Y. Wang[b], Y.Q. Ni[c], J.M. Ko[c]

[a]Department of Mechanics, Zhejiang University, Hangzhou 310027, PR China
[b]Department of Engineering Mechanics, Tsinghua University, Beijing 100084, PR China
[c]Department of Civil and Structural Engineering, The Hong Kong Polytechnic University, Kowloon, Hong Kong

Received 19 May 2008; received in revised form 29 September 2008; accepted 3 October 2008
Handling Editor: L.G. Tham
Available online 17 November 2008

Abstract

The stochastic response of a piezoelectric thick axisymmetric hollow cylinder in plane strain under boundary stochastic excitations is analyzed and calculated. The stochastic stress and electric-potential boundary conditions of the piezoelectric hollow cylinder are converted into homogeneous boundary conditions by transformations that yields the electrical and mechanical coupling partial differential equations of motion with damping and stochastic excitations. The equation for electric potential is integrated radially to obtain the electric potential as a function of displacement, and the displacement is expanded as a series in terms of the Legendre polynomials. The partial differential equation for displacement is further converted into ordinary differential equations by using the Galerkin method, which represent a stochastic multi-degree-of-freedom system with asymmetric stiffness matrix due to the asymmetric electrical and mechanical coupling and the transformed boundary conditions. The frequency-response function matrix and correlation function matrix of the system response are derived from these equations based on the theory of random vibration. The expressions of mean-square displacement and electric potential of the piezoelectric hollow cylinder are finally obtained and illustrated by numerical results for non-white stochastic excitations. The frequency-response characteristics and electrical and mechanical coupling properties are explored.

1. Introduction

Piezoelectric structures as smart sensors or controllers have a potential application in engineering [1]. The free vibration and dynamic characteristics of piezoelectric and composite structures such as beam, plate and shell have been studied extensively [2–12]. The non-homogeneous boundary effects on the electrical and mechanical coupling dynamics were not considered generally. The transient and steady-state vibration responses of piezoelectric and composite structures subjected to external voltage or pressure excitations have been analyzed [13–18]. Several numerical methods for the dynamic response of piezoelectric and composite structures have been presented based on the finite elements, difference equation, Galerkin procedure and

*Corresponding author. Tel.: +86 131 6595 2183.
E-mail address: yingzg@zju.edu.cn (Z.G. Ying).

0022-460X/$ - see front matter © 2008 Elsevier Ltd. All rights reserved.
doi:10.1016/j.jsv.2008.10.002

Laplace transformation [13,19–21]. Much researches on the vibration control of composite structures with piezoelectric material as sensors and controllers have been further made, for instance, the selective modal control, linear quadratic control and bang–bang control [19–27]. Although the results on natural frequencies of the stiffened plate with piezoceramic sensors and actuators in Ref. [9] revealed a slight asymmetry, the non-symmetry dynamics of piezoelectric structure systems have not been recognized and taken into account.

In particular, the piezoelectric shell is regarded as a classical structure and then its dynamics have attracted more attention. The free vibration of piezoelectric ceramic cylinders radially polarized [4–6], the torsional wave motion of a finite inhomogeneous piezoelectric cylindrical shell [28], the axisymmetric and other electroelastic waves of hollow piezoelectric ceramic cylinders [29,30] have been studied. The transient response of axisymmetric piezoelectric hollow cylinders in plane strain has been solved by using the series expansion of Bessel functions and the linear interpolation algorithm [16]. The electrical and mechanical coupling component was implicitly included in a function of time and discretized numerically. The free and forced vibrations of piezoelectric hollow spheres have also been analyzed [7,17,18]. In all those researches, the dynamics problem of piezoelectric structures such as shells with external excitations was assumed as deterministic, except the numerical analysis using the finite element method in Refs. [21,26]. However, a realistic dynamic process of piezoelectric structures as the others inevitably includes random disturbances which can affect the sensing and controlling results. Therefore, the stochastic vibration of piezoelectric structures is a significant research subject.

The present paper focuses on the stochastic response analysis of a piezoelectric axisymmetric hollow cylinder in plane strain. Firstly, the basic equations of the piezoelectric hollow cylinder subjected to boundary stochastic excitations are given. Secondly, the stochastic electric boundary conditions are incorporated in the differential equations of motion by using the transformation of electric potentials, and the equation for electric potential is integrated to obtain the electric potential as a function of displacement. Thirdly, the stochastic stress boundary conditions are converted into homogeneous ones by using the transformation of displacements. Then the displacement is expanded as a series in terms of the Legendre polynomials, and the partial differential equation for displacement is converted into ordinary differential equations according to the Galerkin method, which represent a stochastically excited and damped multi-degree-of-freedom system with asymmetric stiffness. Fourthly, the frequency-response function matrix and correlation function matrix of the system response are derived from these equations based on the theory of random vibration. The expressions of mean-square displacement and electric potential of the piezoelectric hollow cylinder are obtained for non-white stochastic excitations. Finally, numerical results are given to illustrate the stochastic displacement and electric-potential responses of the piezoelectric hollow cylinder to stochastic stress and electric-potential excitations, and their varying with structure and excitation parameters.

2. Basic equations

For an axisymmetric piezoelectric hollow cylinder in plane strain [16] under boundary stochastic excitations, its differential equation of motion in the radius r direction can be expressed as

$$\frac{\partial \sigma_{rr}}{\partial r}+\frac{\sigma_{rr}-\sigma_{\theta\theta}}{r}=\rho\frac{\partial^2 u_r}{\partial t^2}+c_r\frac{\partial u_r}{\partial t} \tag{1}$$

where $\sigma_{rr}=\sigma_{rr}(r,t)$ and $\sigma_{\theta\theta}=\sigma_{\theta\theta}(r,t)$ are, respectively, the radial and circular stresses, $u_r=u_r(r,t)$ is the radial displacement, ρ and c_r are, respectively, the mass density and damping coefficient. The constitutive relations of orthotropic and radially polarized piezoelectric medium are

$$\sigma_{\theta\theta}=c_{11}\gamma_{\theta\theta}+c_{13}\gamma_{rr}+e_{31}\frac{\partial \Phi}{\partial r} \tag{2a}$$

$$\sigma_{rr}=c_{13}\gamma_{\theta\theta}+c_{33}\gamma_{rr}+e_{33}\frac{\partial \Phi}{\partial r} \tag{2b}$$

$$D_r=e_{31}\gamma_{\theta\theta}+e_{33}\gamma_{rr}-\varepsilon_{33}\frac{\partial \Phi}{\partial r} \tag{2c}$$

where $\gamma_{\theta\theta}$ and γ_{rr} are, respectively, the circular and radial strains, c_{ij}, e_{ij} and ε_{ij} $(i,j=1,3)$ are, respectively, elastic, piezoelectric and dielectric constants, $D_r = D_r(r,t)$ is the radial electric displacement, and $\Phi = \Phi(r,t)$ is the electric potential. The strain–displacement relations for the axisymmetric plane strain problem are

$$\gamma_{rr} = \frac{\partial u_r}{\partial r}, \quad \gamma_{\theta\theta} = \frac{u_r}{r} \tag{3a,b}$$

and the other displacements in cylindrical coordinates (r, θ, z) $u_\theta = u_z = 0$. In absence of free charge density, the charge equation of electrostatics is

$$\frac{1}{r}\frac{\partial}{\partial r}(rD_r) = 0 \tag{4}$$

By substituting strains (3) into Eq. (2), Eqs. (1), (2) and (4) can be rewritten in the dimensionless form as follows:

$$\frac{\partial \sigma_r}{\partial \lambda} + \frac{\sigma_r - \sigma_\theta}{\lambda} = \frac{\partial^2 u}{\partial \tau^2} + c\frac{\partial u}{\partial \tau} \tag{5}$$

$$\sigma_\theta = c_1\frac{u}{\lambda} + c_3\frac{\partial u}{\partial \lambda} + e_1\frac{\partial \phi}{\partial \lambda} \tag{6a}$$

$$\sigma_r = c_3\frac{u}{\lambda} + \frac{\partial u}{\partial \lambda} + e_3\frac{\partial \phi}{\partial \lambda} \tag{6b}$$

$$D = e_1\frac{u}{\lambda} + e_3\frac{\partial u}{\partial \lambda} - \frac{\partial \phi}{\partial \lambda} \tag{7}$$

$$\frac{1}{\lambda}\frac{\partial}{\partial \lambda}(\lambda D) = 0 \tag{8}$$

where

$$\sigma_i = \frac{\sigma_{ii}}{c_{33}} \quad (i = r, \theta), \ u = \frac{u_r}{b}, \ D = \frac{D_r}{\sqrt{c_{33}\varepsilon_{33}}}, \ \phi = \frac{\Phi}{b}\sqrt{\frac{\varepsilon_{33}}{c_{33}}}$$

$$\lambda = \frac{r}{b}, \quad \tau = \frac{t}{b}\sqrt{\frac{c_{33}}{\rho}}, \ c = \frac{bc_r}{\sqrt{\rho c_{33}}}, \ c_1 = \frac{c_{11}}{c_{33}}, \ c_3 = \frac{c_{13}}{c_{33}}$$

$$e_1 = \frac{e_{31}}{\sqrt{c_{33}\varepsilon_{33}}}, \quad e_3 = \frac{e_{33}}{\sqrt{c_{33}\varepsilon_{33}}} \tag{9}$$

in which b is the outer radius of the hollow cylinder. The stochastic boundary conditions for stress and electric potential corresponding to Eqs. (5)–(8) are

$$\sigma_r(s,\tau) = \xi_a(\tau), \quad \sigma_r(1,\tau) = \xi_b(\tau) \tag{10a,b}$$

$$\phi(s,\tau) = \eta_a(\tau), \quad \phi(1,\tau) = \eta_b(\tau) \tag{11a,b}$$

where $s = a/b$, a is the inner radius of the hollow cylinder, $\xi_a(\tau)$, $\xi_b(\tau)$, $\eta_a(\tau)$ and $\eta_b(\tau)$ are the independent stochastic processes with power spectral densities $S_{\xi a}(\omega)$, $S_{\xi b}(\omega)$, $S_{\eta a}(\omega)$ and $S_{\eta b}(\omega)$, respectively. The initial displacement and velocity of the cylinder are assumed as zeros.

Substituting stresses (6) into Eq. (5) and electric displacement (7) into Eq. (8) yield the differential equations of motion for displacement u and electric potential ϕ as follows:

$$\frac{\partial^2 u}{\partial \lambda^2} + \frac{1}{\lambda}\frac{\partial u}{\partial \lambda} - c_1\frac{u}{\lambda^2} + e_3\frac{\partial^2 \phi}{\partial \lambda^2} + \frac{e_3 - e_1}{\lambda}\frac{\partial \phi}{\partial \lambda} = \frac{\partial^2 u}{\partial \tau^2} + c\frac{\partial u}{\partial \tau} \tag{12}$$

$$e_3\frac{\partial^2 u}{\partial \lambda^2} + \frac{e_3 + e_1}{\lambda}\frac{\partial u}{\partial \lambda} - \frac{\partial^2 \phi}{\partial \lambda^2} - \frac{1}{\lambda}\frac{\partial \phi}{\partial \lambda} = 0 \tag{13}$$

It can be observed from Eqs. (12) and (13) that the coupling terms of $\partial u/\partial\lambda$ and $\partial\phi/\partial\lambda$ have asymmetric coefficient matrix. In general, those equations need to be converted into the state equations to solve. However, note that Eq. (13) can be integrated directly. The boundary conditions (10) become correspondingly

$$\sigma_r(s,\tau)=\left(c_3\frac{u}{\lambda}+\frac{\partial u}{\partial\lambda}+e_3\frac{\partial\phi}{\partial\lambda}\right)_{\lambda=s}=\xi_a(\tau) \tag{14a}$$

$$\sigma_r(1,\tau)=\left(c_3\frac{u}{\lambda}+\frac{\partial u}{\partial\lambda}+e_3\frac{\partial\phi}{\partial\lambda}\right)_{\lambda=1}=\xi_b(\tau) \tag{14b}$$

3. Electric potential expressions

The following electric potential transformation is introduced:

$$\phi=\frac{1}{1-s}[(1-\lambda)\eta_a+(\lambda-s)\eta_b]+\phi_0 \tag{15}$$

Substituting transformation (15) into Eqs. (12) and (13), yields

$$\frac{\partial^2 u}{\partial\lambda^2}+\frac{1}{\lambda}\frac{\partial u}{\partial\lambda}-c_1\frac{u}{\lambda^2}+e_3\frac{\partial^2\phi_0}{\partial\lambda^2}+\frac{e_3-e_1}{\lambda}\frac{\partial\phi_0}{\partial\lambda}+\frac{e_3-e_1}{\lambda(1-s)}(\eta_b-\eta_a)=\frac{\partial^2 u}{\partial\tau^2}+c\frac{\partial u}{\partial\tau} \tag{16}$$

$$e_3\frac{\partial^2 u}{\partial\lambda^2}+\frac{e_3+e_1}{\lambda}\frac{\partial u}{\partial\lambda}-\frac{\partial^2\phi_0}{\partial\lambda^2}-\frac{1}{\lambda}\frac{\partial\phi_0}{\partial\lambda}-\frac{1}{\lambda(1-s)}(\eta_b-\eta_a)=0 \tag{17}$$

The boundary conditions of electric potential become correspondingly homogeneous, i.e.,

$$\phi_0(s,\tau)=\phi_0(1,\tau)=0 \tag{18}$$

By integrating Eq. (17) with respect to λ and using conditions (18), the electric potential ϕ_0 is expressed by displacement u as follows:

$$\phi_0=e_3\left[u-\overline{u}_b-\frac{\ln\lambda}{\ln s}(\overline{u}_a-\overline{u}_b)\right]+e_1\left[\int_s^\lambda\frac{u}{\lambda}\,\mathrm{d}\lambda-\left(1-\frac{\ln\lambda}{\ln s}\right)\int_s^1\frac{u}{\lambda}\,\mathrm{d}\lambda\right]+(\eta_a-\eta_b)\left[\frac{\ln\lambda}{\ln s}-\frac{1-\lambda}{1-s}\right] \tag{19}$$

where boundary displacements

$$\overline{u}_a=u(s,\tau),\quad \overline{u}_b=u(1,\tau) \tag{20a,b}$$

By using expression (19), Eq. (16) is converted into the following differential equation only for displacement u:

$$\begin{aligned}(1+e_3^2)\frac{\partial^2 u}{\partial\lambda^2}+\frac{1+e_3^2}{\lambda}\frac{\partial u}{\partial\lambda}-(c_1+e_1^2)\frac{u}{\lambda^2}-\frac{e_1^2}{\lambda^2\ln s}\int_s^1\frac{u}{\lambda}\mathrm{d}\lambda-(\eta_a-\eta_b)\frac{e_1}{\lambda^2\ln s}+(\overline{u}_a-\overline{u}_b)\frac{e_1e_3}{\lambda^2\ln s}\\ =\frac{\partial^2 u}{\partial\tau^2}+c\frac{\partial u}{\partial\tau}\end{aligned} \tag{21}$$

The boundary conditions (14) become as

$$\left[(1+e_3^2)\frac{\partial u}{\partial\lambda}+(c_3+e_1e_3)\frac{u}{\lambda}\right]_{\lambda=s}=\xi_1(\tau) \tag{22a}$$

$$\left[(1+e_3^2)\frac{\partial u}{\partial\lambda}+(c_3+e_1e_3)\frac{u}{\lambda}\right]_{\lambda=1}=\xi_2(\tau) \tag{22b}$$

with stochastic processes

$$\xi_1=\xi_a-(\eta_a-\eta_b)\frac{e_3}{s\ln s}-\frac{e_1e_3}{s\ln s}\int_s^1\frac{u}{\lambda}\mathrm{d}\lambda+\frac{e_3^2}{s\ln s}(\overline{u}_a-\overline{u}_b) \tag{23a}$$

$$\xi_2 = \xi_b - (\eta_a - \eta_b)\frac{e_3}{\ln s} - \frac{e_1 e_3}{\ln s}\int_s^1 \frac{u}{\lambda}\mathrm{d}\lambda + \frac{e_3^2}{\ln s}(\overline{u}_a - \overline{u}_b) \tag{23b}$$

Eq. (21) has the coupling terms of coordinate λ and time function such that the separating variable technique cannot be used directly.

4. Displacement transformation and ordinary differential equations

To convert the boundary conditions (22) into homogeneous ones and expand the displacement as a series in radial functions, the following displacement transformation is further introduced:

$$u = A_0(\lambda - 1)^2\xi_1 + B_0(\lambda - s)^2\xi_2 + u_0 \tag{24}$$

where constants

$$A_0 = \frac{1}{2(1+e_3^2)(s-1) + (c_3 + e_1 e_3)(s-1)^2/s} \tag{25a}$$

$$B_0 = \frac{1}{2(1+e_3^2)(1-s) + (c_3 + e_1 e_3)(1-s)^2} \tag{25b}$$

Substituting transformation (24) into Eq. (21) yields the differential equation for displacement u_0 as follows:

$$\begin{aligned}
&(1+e_3^2)\frac{\partial^2 u_0}{\partial\lambda^2} + \frac{1+e_3^2}{\lambda}\frac{\partial u_0}{\partial\lambda} - (c_1 + e_1^2)\frac{u_0}{\lambda^2} - \frac{e_1^2}{\lambda^2\ln s}\int_s^1 \frac{u_0}{\lambda}\mathrm{d}\lambda + \frac{1+e_3^2}{\lambda}[2A_0(2\lambda-1)\xi_1 + 2B_0(2\lambda - s)\xi_2] \\
&- \frac{c_1 + e_1^2}{\lambda^2}[A_0(\lambda-1)^2\xi_1 + B_0(\lambda-s)^2\xi_2] - \frac{e_1^2}{2\lambda^2\ln s}\{A_0[(1-s)(s-3) - 2\ln s]\xi_1 + B_0[(1-s)(1-3s) \\
&- 2s^2\ln s]\xi_2\} + \frac{e_1 e_3}{\lambda^2\ln s}[A_0(1-s)^2\xi_1 - B_0(1-s)^2\xi_2 + \overline{u}_{0a} - \overline{u}_{0b}] - \frac{e_1}{\lambda^2\ln s}(\eta_a - \eta_b) - A_0(\lambda-1)^2 \\
&\times\left(\frac{\partial^2\xi_1}{\partial\tau^2} + c\frac{\partial\xi_1}{\partial\tau}\right) - B_0(\lambda-s)^2\frac{\partial^2\xi_2}{\partial\tau^2} + c\frac{\partial\xi_2}{\partial\tau} = \frac{\partial^2 u_0}{\partial\tau^2} + c\frac{\partial u_0}{\partial\tau}
\end{aligned} \tag{26}$$

where $\overline{u}_{0a} = u_0(s,\tau)$ and $\overline{u}_{0b} = u_0(1,\tau)$ are transformed boundary displacements. The boundary conditions (22) for displacement become correspondingly

$$\left[(1+e_3^2)\frac{\partial u_0}{\partial\lambda} + (c_3 + e_1 e_3)\frac{u_0}{\lambda}\right]_{\lambda=s,1} = 0 \tag{27}$$

The expressions of ξ_1 and ξ_2 are

$$\begin{aligned}
\xi_1 = {}& \xi_a - (\eta_a - \eta_b)\frac{e_3}{s\ln s} - \frac{e_1 e_3}{s\ln s}\int_s^1 \frac{u_0}{\lambda}\mathrm{d}\lambda - \frac{e_1 e_3}{2s\ln s}\{A_0[(1-s)(s-3) - 2\ln s]\xi_1 + B_0[(1-s)(1-3s) \\
&- 2s^2\ln s]\xi_2\} + \frac{e_3^2}{s\ln s}[A_0(1-s)^2\xi_1 - B_0(1-s)^2\xi_2 + \overline{u}_{0a} - \overline{u}_{0b}]
\end{aligned} \tag{28a}$$

$$\begin{aligned}
\xi_2 = {}& \xi_b - (\eta_a - \eta_b)\frac{e_3}{\ln s} - \frac{e_1 e_3}{\ln s}\int_s^1 \frac{u_0}{\lambda}\mathrm{d}\lambda - \frac{e_1 e_3}{2\ln s}\{A_0[(1-s)(s-3) - 2\ln s]\xi_1 + B_0[(1-s)(1-3s) \\
&- 2s^2\ln s]\xi_2\} + \frac{e_3^2}{\ln s}[A_0(1-s)^2\xi_1 - B_0(1-s)^2\xi_2 + \overline{u}_{0a} - \overline{u}_{0b}]
\end{aligned} \tag{28b}$$

Eq. (28) can be solved to obtain ξ_1 and ξ_2, and then the stochastic excitations in Eq. (26) due to the stress boundary conditions are determined. On the left side of Eq. (26), the terms involving e_1 and e_3 stems from the electrical and mechanical coupling, which represent the coupling stiffness.

The Legendre polynomials are used for constructing a series of functions of the radial coordinate, $N_j(\lambda)$, which satisfy the homogeneous boundary conditions (27). Then the displacement u_0 is

expanded as

$$u_0(\lambda,\tau) \cong \sum_{j=1}^{n} N_j(\lambda) q_j(\tau) \tag{29}$$

where $q_j(\tau)$ is a function of time, and the spacial function

$$N_j(\lambda) = p_{j+1}(k_j,-1)P_j(k_j x) - p_j(k_j,-1)P_{j+1}(k_j x) \tag{30}$$

with coefficients

$$p_j(k_j,-1) = \frac{2k_j}{1-s}(1+e_3^2)P_j'(-k_j) + \frac{c_3+e_1e_3}{s}P_j(-k_j) \tag{31a}$$

$$p_{j+1}(k_j,-1) = \frac{2k_j}{1-s}(1+e_3^2)P_{j+1}'(-k_j) + \frac{c_3+e_1e_3}{s}P_{j+1}(-k_j) \tag{31b}$$

in which $P_j(k_j x)$ and $P_{j+1}(k_j x)$ are, respectively, the jth and $j+1$th Legendre polynomials, and the superscript "′" denotes the derivative with respect to $k_j x$. The relationship between variables x and λ is

$$x = \frac{2(\lambda - s)}{1-s} - 1 \tag{32}$$

The constant k_j is determined by the following algebraic equation:

$$p_{j+1}(k_j,-1)p_j(k_j,1) - p_j(k_j,-1)p_{j+1}(k_j,1) = 0 \tag{33}$$

with coefficients

$$p_j(k_j,1) = \frac{2k_j}{1-s}(1+e_3^2)P_j'(k_j) + (c_3+e_1e_3)P_j(k_j) \tag{34a}$$

$$p_{j+1}(k_j,1) = \frac{2k_j}{1-s}(1+e_3^2)P_{j+1}'(k_j) + (c_3+e_1e_3)P_{j+1}(k_j) \tag{34b}$$

It can be obtained that the function $N_j(\lambda)$ satisfies the boundary conditions (27) by substituting Eqs. (29) and (30) into Eq. (27) and using Eq. (33), and $N_1(\lambda) = 0$ due to real constant $k_1 = 0$ by solving Eq. (33) under certain conditions, for instance, $s \geqslant 0.186$.

According to the Galerkin method, substituting displacement (29) into Eq. (26), multiplying Eq. (26) by $\lambda N_i(\lambda)$ and integrating it with respect to λ on $[s,1]$ yield ordinary differential equations for $q_j(\tau)$, which can be rewritten in the following matrix form:

$$\mathbf{M}\ddot{\mathbf{Q}} + \mathbf{C}\dot{\mathbf{Q}} + \mathbf{K}\mathbf{Q} = \mathbf{F}(\tau) \tag{35}$$

where the superscript "." denotes the derivative with respect to τ, generalized coordinate vector $\mathbf{Q}$, generalized mass matrix $\mathbf{M}$, generalized damping matrix $\mathbf{C}$, generalized stiffness matrix $\mathbf{K}$ and generalized stochastic excitation vector $\mathbf{F}$ are, respectively,

$$\mathbf{Q} = \begin{Bmatrix} q_1 \\ q_2 \\ \vdots \\ q_n \end{Bmatrix}, \quad \mathbf{M} = \begin{bmatrix} m_{11} & m_{12} & \cdots & m_{1n} \\ m_{21} & m_{22} & \cdots & m_{2n} \\ \vdots & \vdots & & \vdots \\ m_{n1} & m_{n2} & \cdots & m_{nn} \end{bmatrix}, \quad \mathbf{C} = \begin{bmatrix} c_{11}^d & c_{12}^d & \cdots & c_{1n}^d \\ c_{21}^d & c_{22}^d & \cdots & c_{2n}^d \\ \vdots & \vdots & & \vdots \\ c_{n1}^d & c_{n2}^d & \cdots & c_{nn}^d \end{bmatrix} \tag{36a,b,c}$$

$$\mathbf{K} = \begin{bmatrix} k_{11} & k_{12} & \cdots & k_{1n} \\ k_{21} & k_{22} & \cdots & k_{2n} \\ \vdots & \vdots & & \vdots \\ k_{n1} & k_{n2} & \cdots & k_{nn} \end{bmatrix}, \quad \mathbf{F} = \begin{Bmatrix} f_1 \\ f_2 \\ \vdots \\ f_n \end{Bmatrix} \tag{36d,e}$$

with elements

$$m_{ij} = \int_s^1 \lambda N_i(\lambda)N_j(\lambda)\,\mathrm{d}\lambda - \int_s^1 \frac{N_j(\lambda)}{\lambda}\mathrm{d}\lambda \cdot \int_s^1 \left[\frac{A_0(\lambda-1)^2}{A_1B_2-A_2B_1}\left(\frac{e_1e_3}{s\ln s}B_2 - \frac{e_1e_3}{\ln s}B_1\right) + \frac{B_0(\lambda-s)^2}{A_1B_2-A_2B_1} \times \left(\frac{e_1e_3}{\ln s}A_1 - \frac{e_1e_3}{s\ln s}A_2\right)\right]\lambda N_i(\lambda)\,\mathrm{d}\lambda + [N_j(s)-N_i(1)]\int_s^1 \left[\frac{A_0(\lambda-1)^2}{A_1B_2-A_2B_1}\cdot\left(\frac{e_3^2}{s\ln s}B_2 - \frac{e_3^2}{\ln s}B_1\right) + \frac{B_0(\lambda-s)^2}{A_1B_2-A_2B_1}\left(\frac{e_3^2}{\ln s}A_1 - \frac{e_3^2}{s\ln s}A_2\right)\right]\lambda N_i(\lambda)\,\mathrm{d}\lambda \tag{37a}$$

$$k_{ij} = \int_s^1 \frac{c_1+e_1^2}{\lambda}N_i(\lambda)N_j(\lambda)\,\mathrm{d}\lambda + (1+e_3^2)\int_s^1 \lambda N_i'(\lambda)N_j'(\lambda)\,\mathrm{d}\lambda - (1+e_3^2)[N_i(1)N_j'(1) - N_i(s)N_j'(s)] + \int_s^1 \frac{N_i(\lambda)}{\lambda}\mathrm{d}\lambda \cdot \left\{\frac{e_1^2}{\ln s}\int_s^1 \frac{N_j(\lambda)}{\lambda}\mathrm{d}\lambda - \frac{e_1e_3}{\ln s}[N_j(s)-N_j(1)]\right\} + [N_j(s)-N_j(1)]\cdot\int_s^1 \left\{\left[(c_1+e_1^2)\frac{(\lambda-1)^2}{\lambda} - 2(1+e_3^2)(2\lambda-1) + \frac{e_1^2}{2\lambda\ln s}((1-s)(s-3) - 2\ln s) - \frac{e_1e_3}{\lambda\ln s}(1-s)^2\right]\frac{A_0}{A_1B_2-A_2B_1}\left(\frac{e_3^2}{s\ln s}B_2 - \frac{e_3^2}{\ln s}B_1\right) + \left[(c_1+e_1^2)\frac{(\lambda-s)^2}{\lambda} - 2(1+e_3^2)(2\lambda-s) + \frac{e_1^2}{2\lambda\ln s}((1-s)(1-3s) - 2s^2\ln s) + \frac{e_1e_3}{\lambda\ln s}(1-s)^2\right] \times \frac{B_0}{A_1B_2-A_2B_1}\left(\frac{e_3^2}{\ln s}A_1 - \frac{e_3^2}{s\ln s}A_2\right)\right\}N_i(\lambda)\,\mathrm{d}\lambda - \int_s^1 \frac{N_j(\lambda)}{\lambda}\mathrm{d}\lambda\cdot\int_s^1 \left\{\left[(c_1+e_1^2)\frac{(\lambda-1)^2}{\lambda} - 2(1+e_3^2) \times (2\lambda-1) + \frac{e_1^2}{2\lambda\ln s}((1-s)(s-3) - 2\ln s) - \frac{e_1e_3}{\lambda\ln s}(1-s)^2\right]\frac{A_0}{A_1B_2-A_2B_1}\left(\frac{e_1e_3}{s\ln s}B_2 - \frac{e_1e_3}{\ln s}B_1\right) + \left[(c_1+e_1^2)\frac{(\lambda-s)^2}{\lambda} - 2(1+e_3^2)(2\lambda-s) + \frac{e_1^2}{2\lambda\ln s}((1-s)(1-3s) - 2s^2\ln s) + \frac{e_1e_3}{\lambda\ln s}(1-s)^2\right] \times \frac{B_0}{A_1B_2-A_2B_1}\left(\frac{e_1e_3}{\ln s}A_1 - \frac{e_1e_3}{s\ln s}A_2\right)\right\}N_i(\lambda)\,\mathrm{d}\lambda \tag{37b}$$

$$f_i = [(\ddot{\eta}_a - \ddot{\eta}_b) + c(\dot{\eta}_a - \dot{\eta}_b)]\int_s^1 \left[\frac{A_0(\lambda-1)^2}{A_1B_2-A_2B_1}\left(\frac{e_3}{s\ln s}B_2 - \frac{e_3}{\ln s}B_1\right) + \frac{B_0(\lambda-s)^2}{A_1B_2-A_2B_1}\left(\frac{e_3}{s\ln s}A_1 - \frac{e_3}{\ln s}A_2\right)\right] \times \lambda N_i(\lambda)\,\mathrm{d}\lambda - \int_s^1 \left[\frac{A_0(\lambda-1)^2}{A_1B_2-A_2B_1}(B_2\ddot{\xi}_a + cB_2\dot{\xi}_a - B_1\ddot{\xi}_b - cB_1\dot{\xi}_b) - \frac{B_0(\lambda-s)^2}{A_1B_2-A_2B_1}(A_2\ddot{\xi}_a + cA_2\dot{\xi}_a - A_1\ddot{\xi}_b - cA_1\dot{\xi}_b)\right]\lambda N_i(\lambda)\,\mathrm{d}\lambda - (\eta_a-\eta_b)\frac{e_1}{\ln s}\int_s^1 \frac{N_i(\lambda)}{\lambda}\mathrm{d}\lambda + (\eta_a-\eta_b)\int_s^1 \left\{\left[(c_1+e_1^2)\frac{(\lambda-1)^2}{\lambda} - 2(1 + e_3^2)(2\lambda-1) + \frac{e_1^2}{2\lambda\ln s}((1-s)(s-3) - 2\ln s) - \frac{e_1e_3}{\lambda\ln s}(1-s)^2\right]\frac{A_0}{A_1B_2-A_2B_1}\left(\frac{e_3}{s\ln s}B_2 - \frac{e_3}{\ln s}B_1\right) + \left[(c_1+e_1^2)\frac{(\lambda-s)^2}{\lambda} - 2(1+e_3^2)(2\lambda-s) + \frac{e_1^2}{2\lambda\ln s}((1-s)(1-3s) - 2s^2\ln s) + \frac{e_1e_3}{\lambda\ln s}(1-s)^2\right] \times \frac{B_0}{A_1B_2-A_2B_1}\left(\frac{e_3}{\ln s}A_1 - \frac{e_3}{s\ln s}A_2\right)\right\}N_i(\lambda)\,\mathrm{d}\lambda - \int_s^1 \left\{\left[(c_1+e_1^2)\frac{(\lambda-1)^2}{\lambda} - 2(1+e_3^2) \times (2\lambda-1) + \frac{e_1^2}{2\lambda\ln s}((1-s)(s-3) - 2\ln s) - \frac{e_1e_3}{\lambda\ln s}(1-s)^2\right]\frac{A_0(B_2\xi_a - B_1\xi_b)}{A_1B_2-A_2B_1} - \left[(c_1+e_1^2)\frac{(\lambda-s)^2}{\lambda} - 2(1+e_3^2)(2\lambda-s) + \frac{e_1^2}{2\lambda\ln s}((1-s)(1-3s) - 2s^2\ln s) + \frac{e_1e_3}{\lambda\ln s}(1-s)^2\right]\frac{B_0(A_2\xi_a - A_1\xi_b)}{A_1B_2-A_2B_1}\right\}N_i(\lambda)\,\mathrm{d}\lambda \tag{37c}$$

$$c_{ij}^d = cm_{ij} \tag{37d}$$

Eq. (35) represents a multi-degree-of-freedom system subjected to stochastic excitations. This system has asymmetric stiffness and mass matrices due to the boundary excitations and the electrical and mechanical

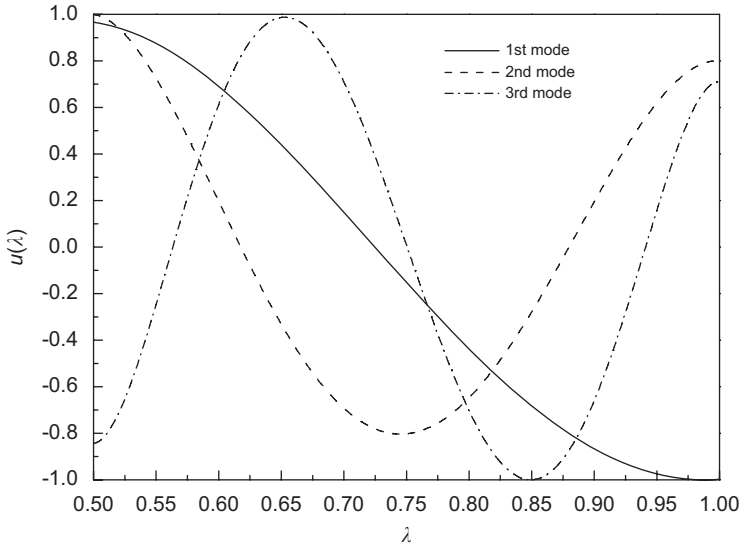

Fig. 1. Vibration modes.

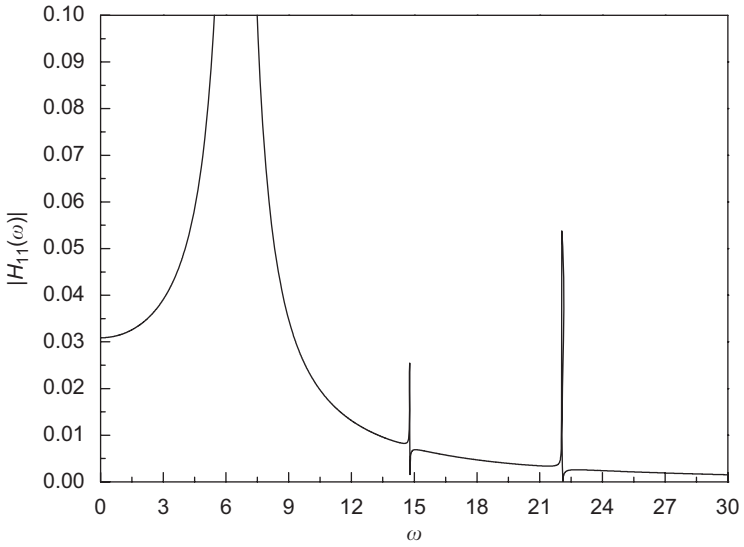

Fig. 2. Frequency-response function without damping $H_{11}(\omega)$.

coupling. Therefore, the conventional modal superposition method for symmetric systems is not usable to the asymmetric system.

5. Stochastic response

The stochastic response of the asymmetric linear multi-degree-of-freedom system (35) can be estimated by using the relationship between the correlation function in time domain and the power spectral density in frequency domain. The frequency-response function matrix of the system (35) is

$$\mathbf{H}(\mathrm{j}\omega) = (\mathbf{K} + \mathrm{j}\omega\mathbf{C} - \omega^2\mathbf{M})^{-1} \tag{38}$$

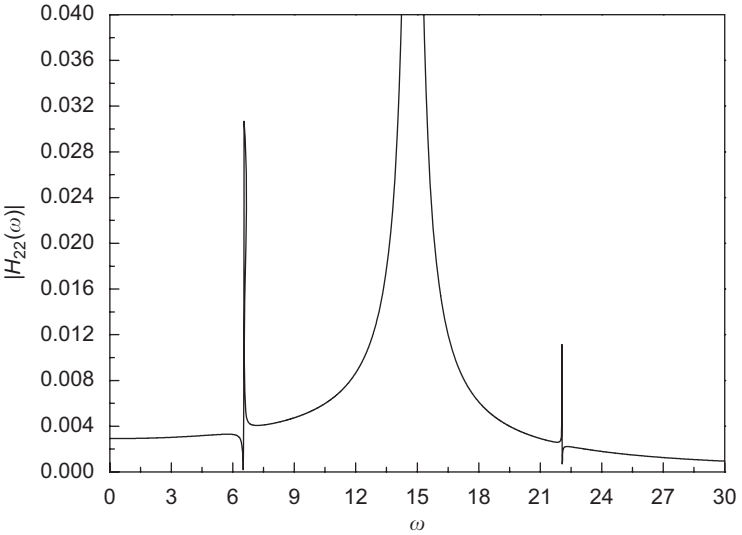

Fig. 3. Frequency-response function without damping $H_{22}(\omega)$.

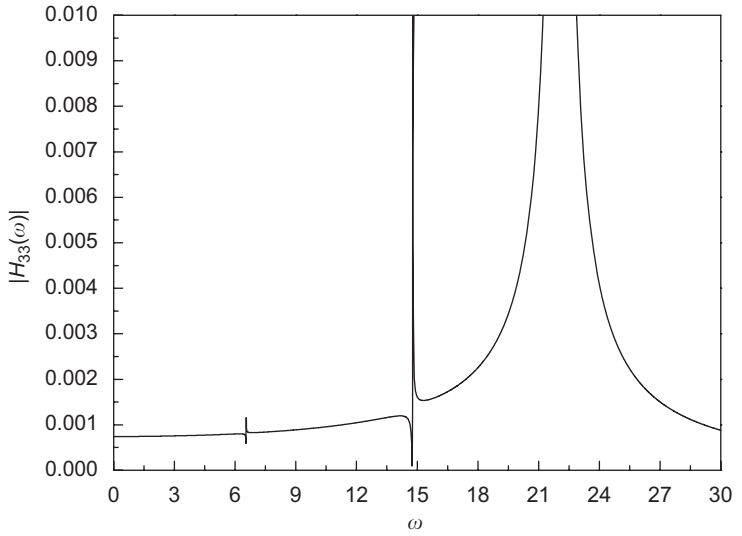

Fig. 4. Frequency-response function without damping $H_{33}(\omega)$.

where ω is a frequency and $\mathrm{j} = \sqrt{-1}$. Then the power spectral density matrix of the system response is correspondingly

$$\mathbf{S}_Q(\omega) = \mathbf{H}(\mathrm{j}\omega)\mathbf{S}_F(\omega)\mathbf{H}^{\mathrm{T}}(\mathrm{j}\omega) \tag{39}$$

where $\mathbf{S}_F(\omega)$ is the power spectral density matrix of the stochastic excitation $\mathbf{F}(\tau)$, and the superscript "T" denotes the conjugation and transposition operation of a matrix. Rewrite Eq. (37c) as

$$f_i(\tau) = C_{1i}\xi_a(\tau) + D_{1i}\xi_b(\tau) + C_{2i}\dot{\xi}_a(\tau) + D_{2i}\dot{\xi}_b(\tau) + C_{3i}\ddot{\xi}_a(\tau) + D_{3i}\ddot{\xi}_b(\tau) + C_{4i}\eta_a(\tau) + D_{4i}\eta_b(\tau) + C_{5i}\dot{\eta}_a(\tau) + D_{5i}\dot{\eta}_b(\tau) + C_{6i}\ddot{\eta}_a(\tau) + D_{6i}\ddot{\eta}_b(\tau) \tag{40}$$

where constants C_{li} and D_{li} $(l = 1,2,\ldots,6)$ can be determined by comparing Eqs. (40) and (37c). For independent stationary non-white stochastic boundary excitations $\xi_a(\tau)$, $\xi_b(\tau)$, $\eta_a(\tau)$ and $\eta_b(\tau)$ with,

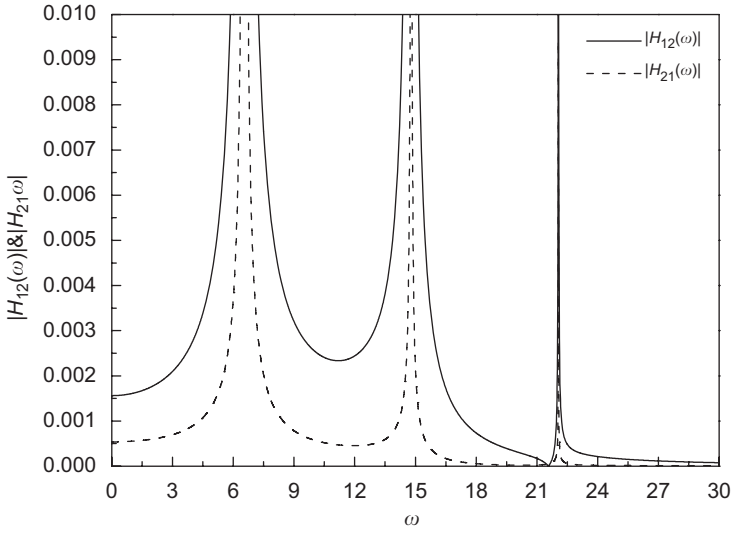

Fig. 5. Frequency-response functions without damping $H_{12}(\omega)$ and $H_{21}(\omega)$.

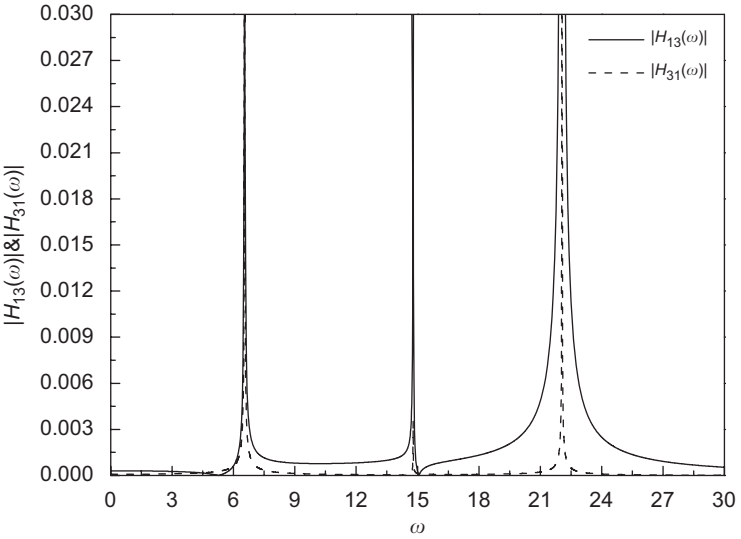

Fig. 6. Frequency-response functions without damping $H_{13}(\omega)$ and $H_{31}(\omega)$.

respectively, power spectral densities $S_{\xi a}(\omega)$, $S_{\xi b}(\omega)$, $S_{\eta a}(\omega)$ and $S_{\eta b}(\omega)$, the element in the power spectral density matrix $\mathbf{S}_{\boldsymbol{F}}(\omega)$ of the system excitation is

$$
\begin{aligned}
[\mathbf{S}_{\boldsymbol{F}}(\omega)]_{ik} = \sum_{l=1,4} \Bigg\{ & [C_{li}C_{lk} + (C_{l+1,i}C_{l+1,k} - C_{li}C_{l+2,k} - C_{l+2,i}C_{lk})\omega^2 + C_{l+2,i}C_{l+2,k}\omega^4 + (C_{li}C_{l+1,k} \\
& - C_{l+1,i}C_{lk})\mathrm{j}\omega + (C_{l+1,i}C_{l+2,k} - C_{l+2,i}C_{l+1,k})\mathrm{j}\omega^3] \left[\frac{1+(-1)^{i-1}}{2} S_{\xi a}(\omega) + \frac{1+(-1)^{i}}{2} S_{\eta a}(\omega) \right] \\
& + [D_{li}D_{lk} + (D_{l+1,i}D_{l+1,k} - D_{li}D_{l+2,k} - D_{l+2,i}D_{lk})\omega^2 + D_{l+2,i}D_{l+2,k}\omega^4 + (D_{li}D_{l+1,k} - D_{l+1,i}D_{lk})\mathrm{j}\omega \\
& + (D_{l+1,i}D_{l+2,k} - D_{l+2,i}D_{l+1,k})\mathrm{j}\omega^3] \left[\frac{1+(-1)^{i-1}}{2} S_{\xi b}(\omega) + \frac{1+(-1)^{i}}{2} S_{\eta b}(\omega) \right] \Bigg\}
\end{aligned} \tag{41}
$$

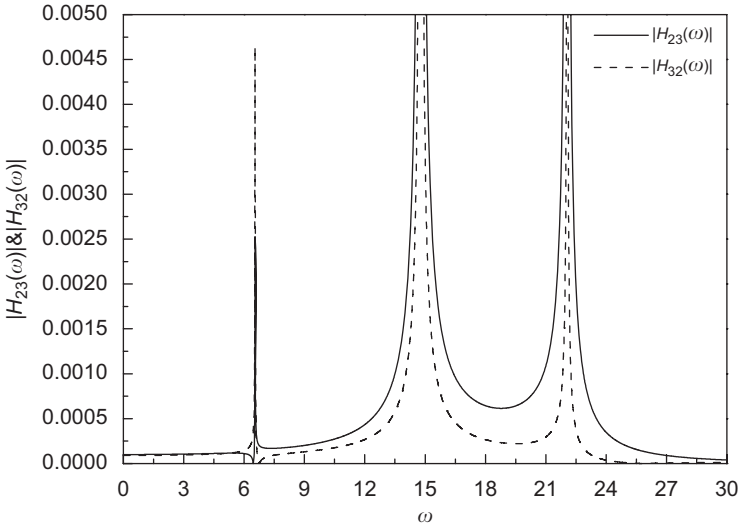

Fig. 7. Frequency-response functions without damping $H_{23}(\omega)$ and $H_{32}(\omega)$.

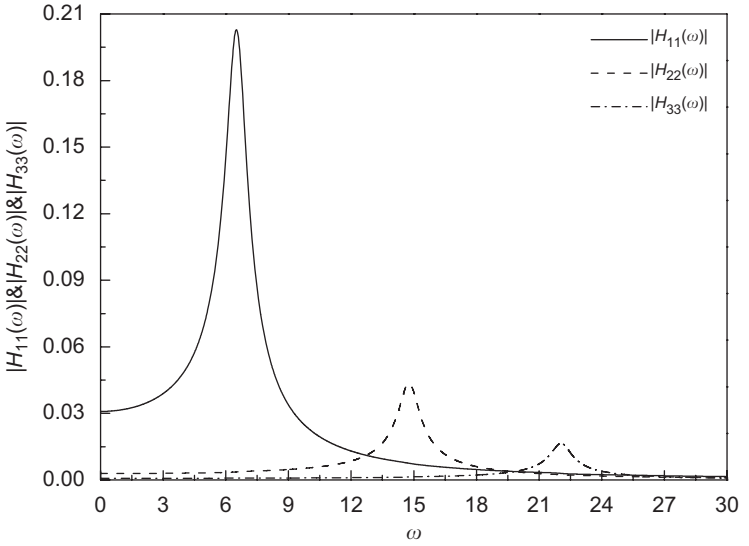

Fig. 8. Damped frequency-response functions $H_{11}(\omega)$, $H_{22}(\omega)$ and $H_{33}(\omega)$.

The natural frequencies of system (35) or the piezoelectric hollow cylinder can be obtained by the peak-value characteristics of the frequency-response function matrix $\mathbf{H}(\mathrm{j}\omega)$, and the response spectrum is determined by the power spectral density matrix $\mathbf{S}_{\boldsymbol{Q}}(\omega)$. The correlation function matrix of the system response $\mathbf{Q}$ can be expressed as

$$\mathbf{R}_{\boldsymbol{Q}}(0) = \int_{-\infty}^{\infty} \mathbf{S}_{\boldsymbol{Q}}(\omega)\,\mathrm{d}\omega \tag{42}$$

The mean-square response $E[q_i^2]$ of the multi-degree-of-freedom system (35) is determined by the diagonal elements of the correlation function matrix $\mathbf{R}_{\boldsymbol{Q}}(0)$. By using Eqs. (29) and (42), the mean-square transformed

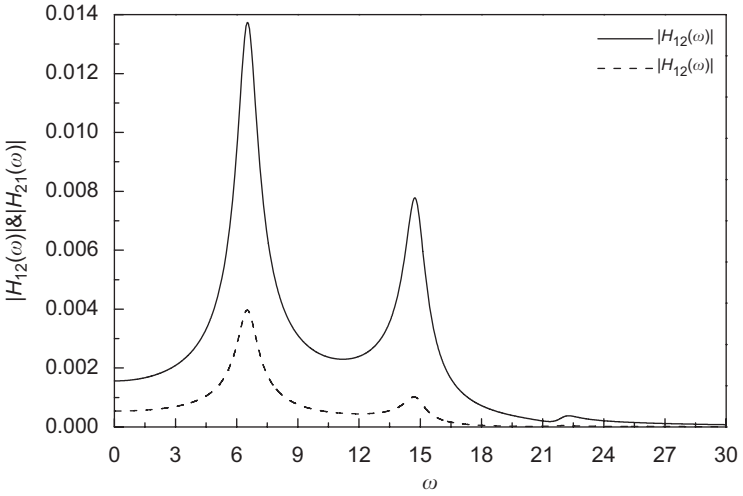

Fig. 9. Damped frequency-response functions $H_{12}(\omega)$ and $H_{21}(\omega)$.

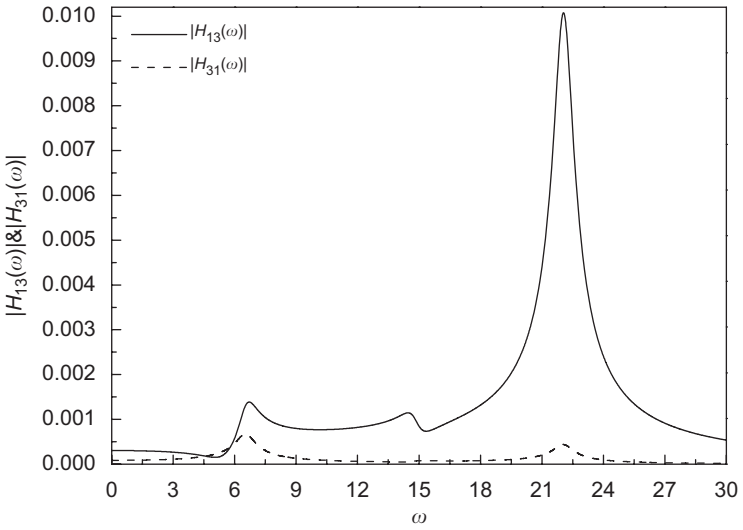

Fig. 10. Damped frequency-response functions $H_{13}(\omega)$ and $H_{31}(\omega)$.

displacement of the piezoelectric hollow cylinder can be obtained as

$$E[u_0^2](\lambda) \cong \sum_{i=1}^{n}\sum_{j=1}^{n} N_i(\lambda)[\mathbf{R}_{\boldsymbol{Q}}(0)]_{ij}N_j(\lambda) \tag{43}$$

Further, substitute Eq. (29) and ξ_1 and ξ_2 from Eq. (28) into Eq. (24), and rewrite it as

$$u(\lambda,\tau) = C_1(\lambda)\xi_a(\tau) + C_2(\lambda)\xi_b(\tau) + C_3(\lambda)\eta_a(\tau) + C_4(\lambda)\eta_b(\tau) + \sum_{i=1}^{n} D_i(\lambda)q_i(\tau) \tag{44}$$

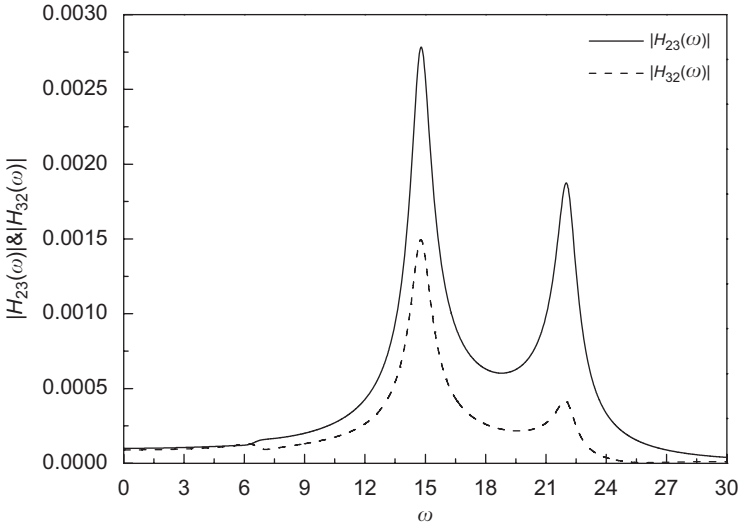

Fig. 11. Damped frequency-response functions $H_{23}(\omega)$ and $H_{32}(\omega)$.

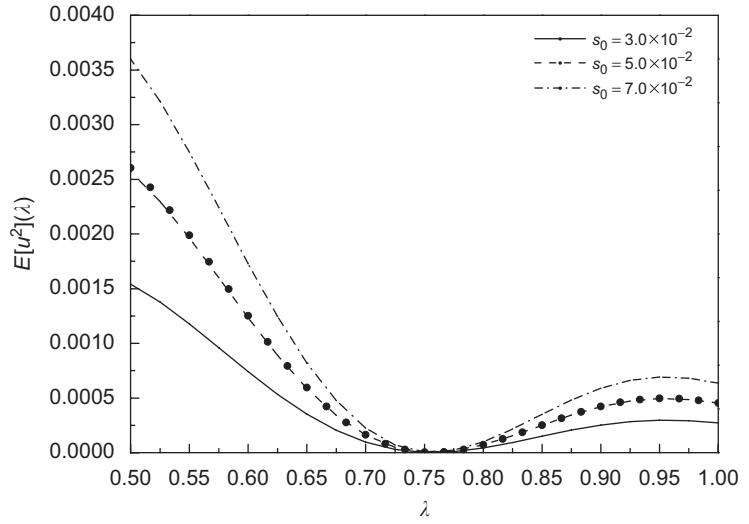

Fig. 12. Mean-square radial displacement $E[u^2]$ versus radial coordinate λ for different boundary pressure intensity s_0 (● by numerical simulation).

where coefficients $C_i(\lambda)$ ($i = 1,2,3,4$) and $D_i(\lambda)$ ($i = 1,2,\ldots,n$) are determined by comparing Eqs. (44) and (24). Then the power spectral density function of the structural displacement response is

$$\begin{aligned} S_u(\lambda,\omega) = {} & C_1^2(\lambda)S_{\xi a}(\omega) + C_2^2(\lambda)S_{\xi b}(\omega) + C_3^2(\lambda)S_{\eta a}(\omega) + C_4^2(\lambda)S_{\eta b}(\omega) + \sum_{i=1}^{n} D_i(\lambda)\{C_1(\lambda)[\mathbf{S}_{\boldsymbol{Q}\xi a}(\omega) \\ & + \mathbf{S}_{\boldsymbol{Q}\xi a}(-\omega)]_i + C_2(\lambda)[\mathbf{S}_{\boldsymbol{Q}\xi b}(\omega) + \mathbf{S}_{\boldsymbol{Q}\xi b}(-\omega)]_i + C_3(\lambda)[\mathbf{S}_{\boldsymbol{Q}\eta a}(\omega) + \mathbf{S}_{\boldsymbol{Q}\eta a}(-\omega)]_i \\ & + C_4(\lambda)[\mathbf{S}_{\boldsymbol{Q}\eta b}(\omega) + \mathbf{S}_{\boldsymbol{Q}\eta b}(-\omega)]_i\} + \sum_{i=1}^{n}\sum_{j=1}^{n} D_i(\lambda)D_j(\lambda)[\mathbf{S}_{\boldsymbol{Q}}(\omega)]_{ij} \end{aligned} \tag{45}$$

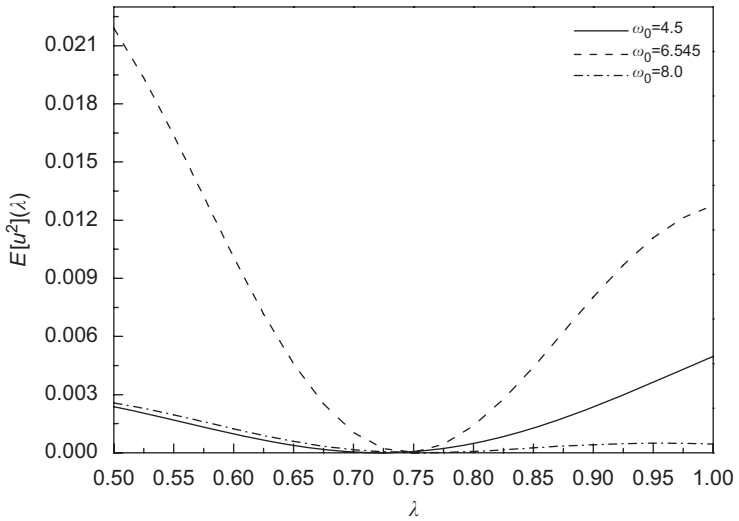

Fig. 13. Mean-square radial displacement $E[u^2]$ versus radial coordinate λ for different boundary-pressure dominant frequency ω_0 around the 1st natural frequency ω_1 ($s_0 = 0.05$).

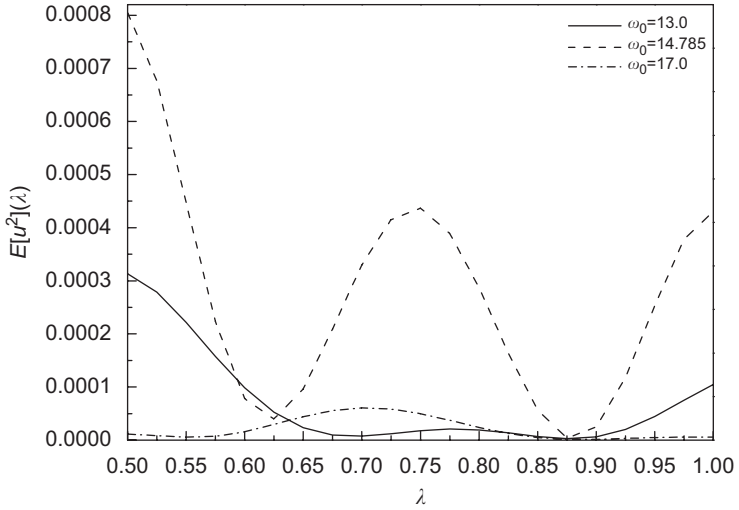

Fig. 14. Mean-square radial displacement $E[u^2]$ versus radial coordinate λ for different boundary-pressure dominant frequency ω_0 around the 2nd natural frequency ω_2 ($s_0 = 0.05$).

where the cross power spectral density vectors of the system response $\mathbf{Q}$ and boundary excitations ξ_a, ξ_b, η_a and η_b as follows:

$$\mathbf{S}_{\boldsymbol{Q}\xi a}(\omega) = \mathbf{H}(-\mathrm{j}\omega)\mathbf{S}_{\boldsymbol{F}\xi a}(\omega), \quad \mathbf{S}_{\boldsymbol{Q}\xi b}(\omega) = \mathbf{H}(-\mathrm{j}\omega)\mathbf{S}_{\boldsymbol{F}\xi b}(\omega) \tag{46a,b}$$

$$\mathbf{S}_{\boldsymbol{Q}\eta a}(\omega) = \mathbf{H}(-\mathrm{j}\omega)\mathbf{S}_{\boldsymbol{F}\eta a}(\omega), \quad \mathbf{S}_{\boldsymbol{Q}\eta b}(\omega) = \mathbf{H}(-\mathrm{j}\omega)\mathbf{S}_{\boldsymbol{F}\eta b}(\omega) \tag{46c,d}$$

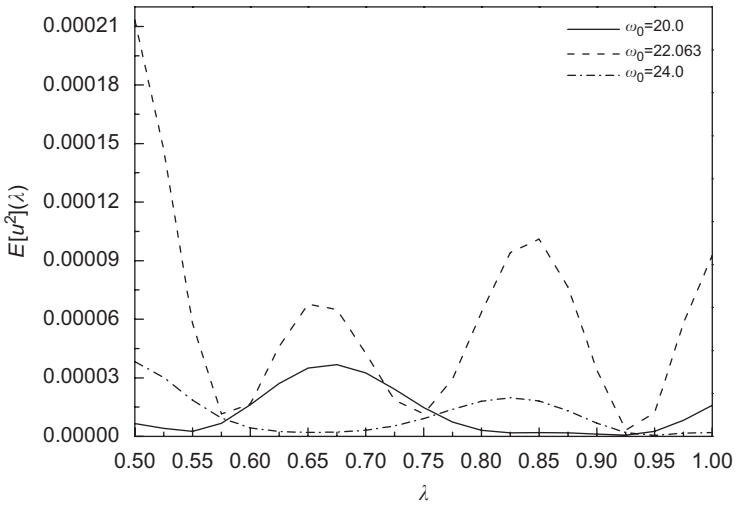

Fig. 15. Mean-square radial displacement $E[u^2]$ versus radial coordinate λ for different boundary-pressure dominant frequency ω_0 around the 3rd natural frequency ω_3 ($s_0 = 0.05$).

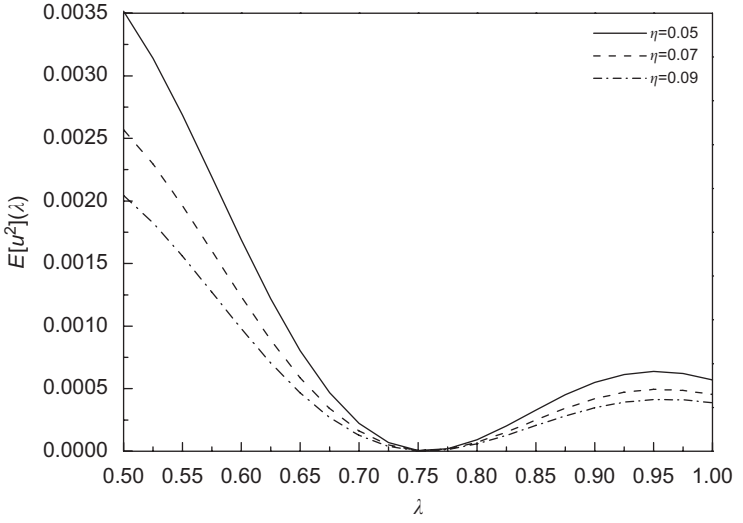

Fig. 16. Mean-square radial displacement $E[u^2]$ versus radial coordinate λ for different boundary-pressure damping coefficient η ($s_0 = 0.05$).

with the elements of the power spectral density vectors of the system boundary excitations

$$[\mathbf{S}_{\boldsymbol{F}\xi a}(\omega)]_i = (C_{1i} - \mathrm{j}\omega C_{2i} - \omega^2 C_{3i}) S_{\xi a}(\omega) \tag{47a}$$

$$[\mathbf{S}_{\boldsymbol{F}\xi b}(\omega)]_i = (D_{1i} - \mathrm{j}\omega D_{2i} - \omega^2 D_{3i}) S_{\xi b}(\omega) \tag{47b}$$

$$[\mathbf{S}_{\boldsymbol{F}\eta a}(\omega)]_i = (C_{4i} - \mathrm{j}\omega C_{5i} - \omega^2 C_{6i}) S_{\eta a}(\omega) \tag{47c}$$

$$[\mathbf{S}_{\boldsymbol{F}\eta b}(\omega)]_i = (D_{4i} - \mathrm{j}\omega D_{5i} - \omega^2 D_{6i}) S_{\eta b}(\omega) \tag{47d}$$

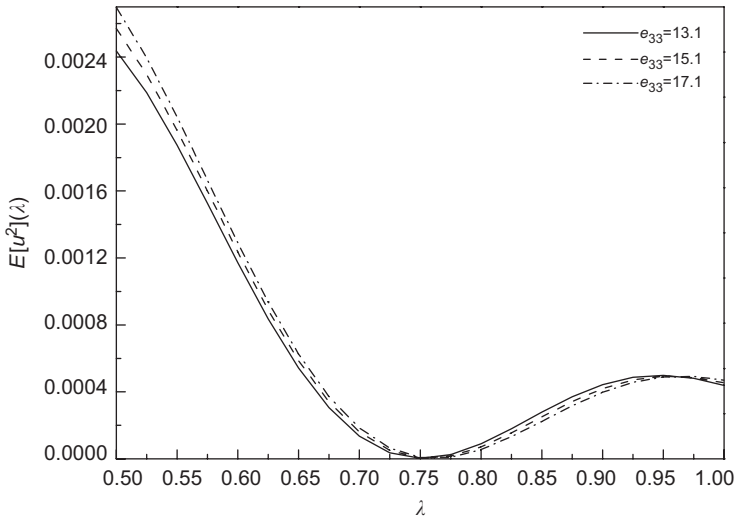

Fig. 17. Mean-square radial displacement $E[u^2]$ versus radial coordinate λ for different piezoelectric constant e_{33} ($s_0 = 0.05$).

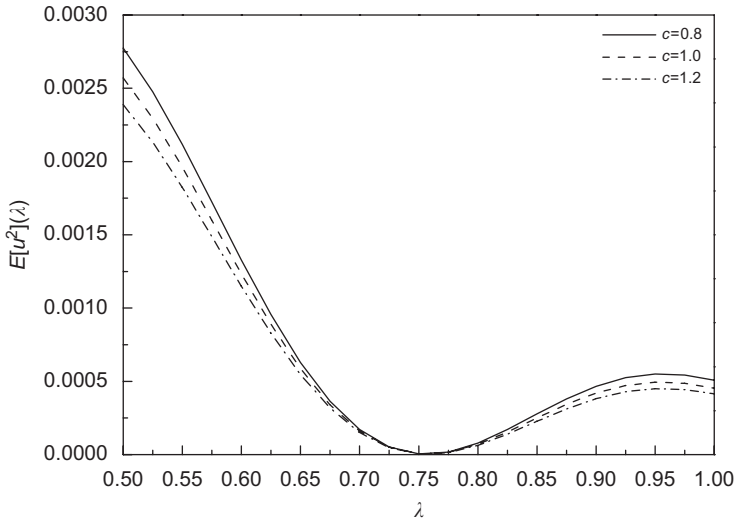

Fig. 18. Mean-square radial displacement $E[u^2]$ versus radial coordinate λ for different structural damping coefficient c ($s_0 = 0.05$).

By using Eqs. (44) and (45), the displacement correlation function or the mean-square displacement of the piezoelectric hollow cylinder can be expressed as

$$E[u^2](\lambda) = R_u(\lambda, 0) = \int_{-\infty}^{+\infty} S_u(\lambda, \omega)\,\mathrm{d}\omega \tag{48}$$

Based on expressions (19) and (15), Eqs. (38), (39), (45) and (46), the power spectral density function, correlation function and mean-square value of the electric potential of the piezoelectric hollow cylinder can be obtained similarly. Eqs. (43) and (48) represent the mean-square displacements (as well as the mean-square electric potentials) as functions of dimensionless radial coordinate λ, which can be used for exploring the

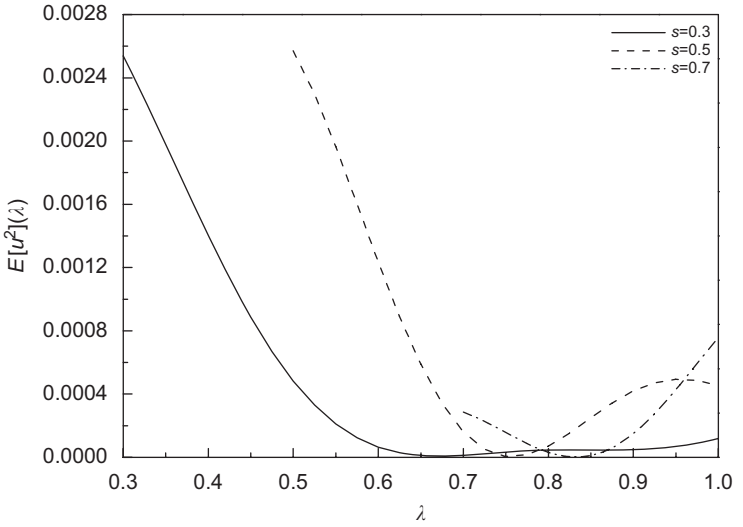

Fig. 19. Mean-square radial displacement $E[u^2]$ versus radial coordinate λ for different ratio s of inner to outer radii ($s_0 = 0.05$).

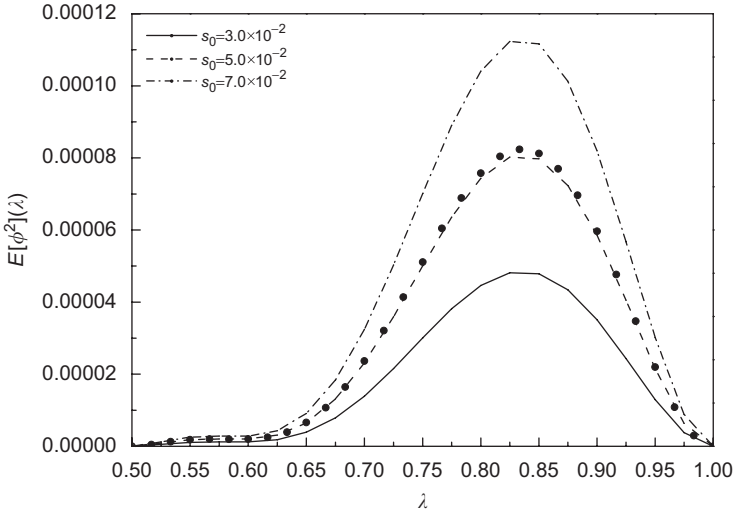

Fig. 20. Mean-square electric potential $E[\phi^2]$ versus radial coordinate λ for different boundary pressure intensity s_0 (● by numerical simulation).

response characteristics to boundary stochastic excitations and the electrical and mechanical coupling properties of the piezoelectric hollow cylinder.

6. Numerical results

For the PZT-4 piezoelectric axisymmetric hollow cylinder subjected to boundary stationary stochastic pressures and electric potentials with structural parameters [31] $c_{11} = 139.0\,\text{GPa}$, $c_{13} = 74.3\,\text{GPa}$, $c_{33} = 115.0\,\text{GPa}$, $e_{31} = -5.2\,\text{C/m}^2$, $e_{33} = 15.1\,\text{C/m}^2$, $\varepsilon_{33} = 5.62 \times 10^{-9}\,\text{C}^2/\text{N m}^2$, $s = a/b = 0.5$, $c = 1.0$ and

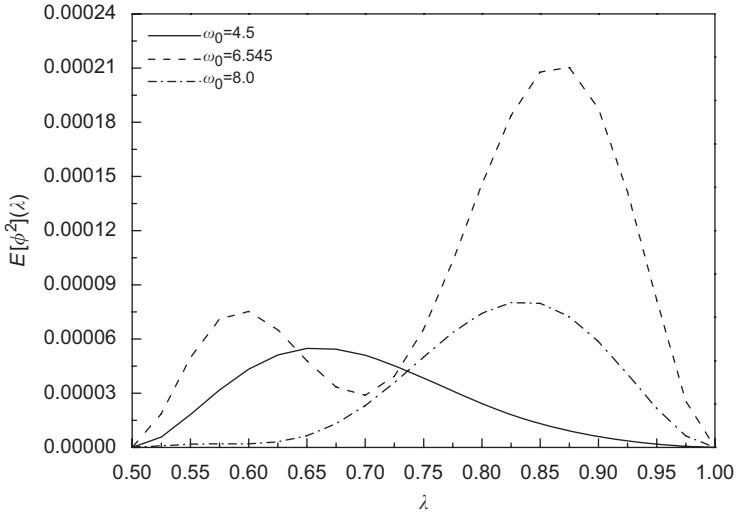

Fig. 21. Mean-square electric potential $E[\phi^2]$ versus radial coordinate λ for different boundary-pressure dominant frequency ω_0 around the 1st natural frequency ω_1 ($s_0 = 0.05$).

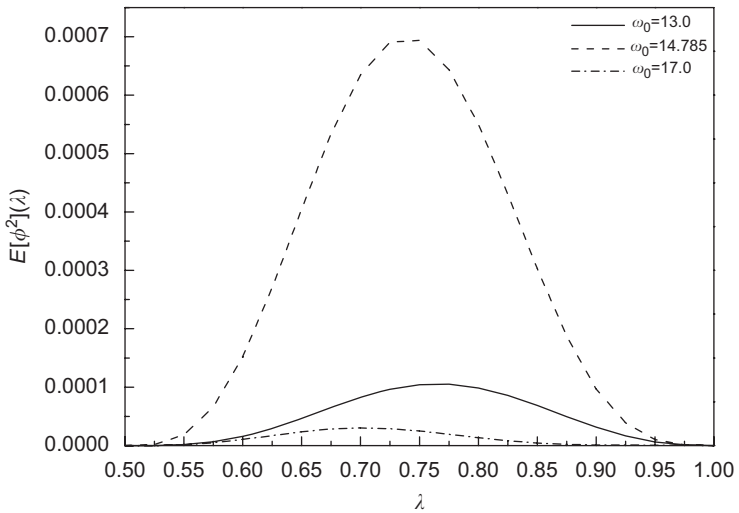

Fig. 22. Mean-square electric potential $E[\phi^2]$ versus radial coordinate λ for different boundary-pressure dominant frequency ω_0 around the 2nd natural frequency ω_2 ($s_0 = 0.05$).

excitation parameters $S_{\xi a}(\omega) = S_{\eta a}(\omega) = 0$,

$$S_{\xi b}(\omega) = \frac{s_0}{(\omega_0^2 - \omega^2)^2 + (2\eta\omega)^2}, \quad S_{\eta b}(\omega) = 0 \tag{49}$$

or

$$S_{\xi b}(\omega) = 0, \quad S_{\eta b}(\omega) = \frac{s_0}{(\omega_0^2 - \omega^2)^2 + (2\eta\omega)^2} \tag{50}$$

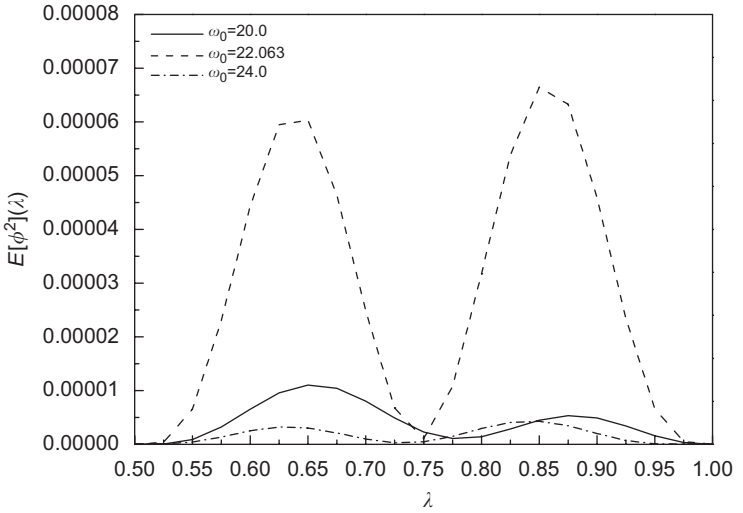

Fig. 23. Mean-square electric potential $E[\phi^2]$ versus radial coordinate λ for different boundary-pressure dominant frequency ω_0 around the 3rd natural frequency ω_3 ($s_0 = 0.05$).

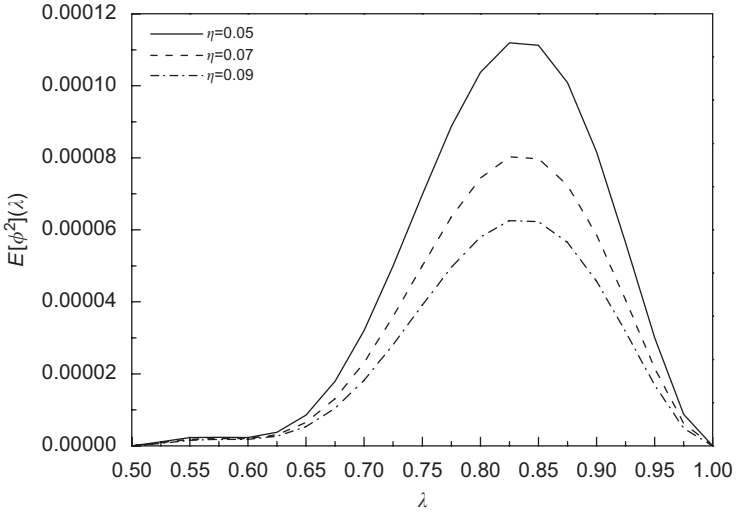

Fig. 24. Mean-square electric potential $E[\phi^2]$ versus radial coordinate λ for different boundary-pressure damping coefficient η ($s_0 = 0.05$).

in which $\omega_0 = 8.0$ and $\eta = 0.07$, numerical results on the vibration modes, frequency-response functions, mean-square displacements and mean-square electric potentials have been obtained and shown in Figs. 1–37.

Figs. 2–7 illustrate the frequency-response functions $H_{11}(\omega)$, $H_{22}(\omega)$, $H_{33}(\omega)$, $H_{12}(\omega)$, $H_{21}(\omega)$, $H_{13}(\omega)$, $H_{31}(\omega)$, $H_{23}(\omega)$ and $H_{32}(\omega)$ in matrix $\mathbf{H}(\omega)$ varying with frequency ω on the interval [0,30] for the piezoelectric hollow cylinder without damping, respectively. It can be seen that the first three natural frequencies are $\omega_1 = 6.545$ ($4.08/b$ Hz), $\omega_2 = 14.785$ ($9.21/b$ Hz) and $\omega_3 = 22.063$ ($13.75/b$ Hz), which are in agreement with the results given in Ref. [4]. The corresponding vibration modes are shown in Fig. 1 in terms of the right eigen-problem. The domains of the natural frequencies ω_1, ω_2 and ω_3 are dominant in the frequency-response functions $H_{11}(\omega)$, $H_{22}(\omega)$ and $H_{33}(\omega)$, respectively. The frequency-response functions $H_{12}(\omega)$ and $H_{21}(\omega)$,

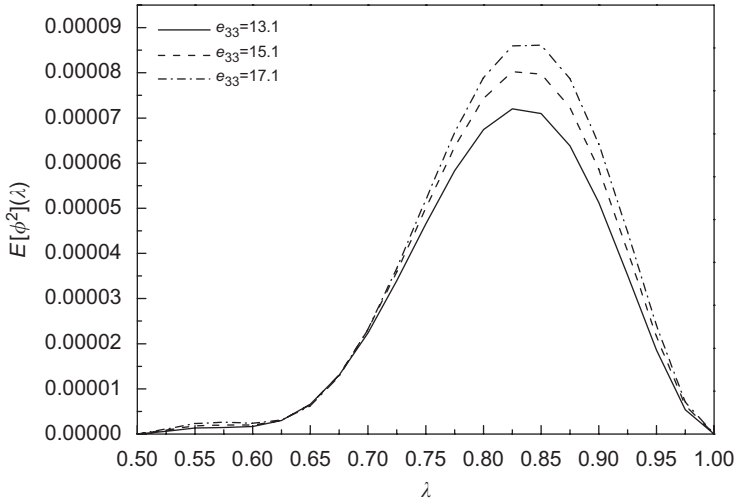

Fig. 25. Mean-square electric potential $E[\phi^2]$ versus radial coordinate λ for different piezoelectric constant e_{33} ($s_0 = 0.05$).

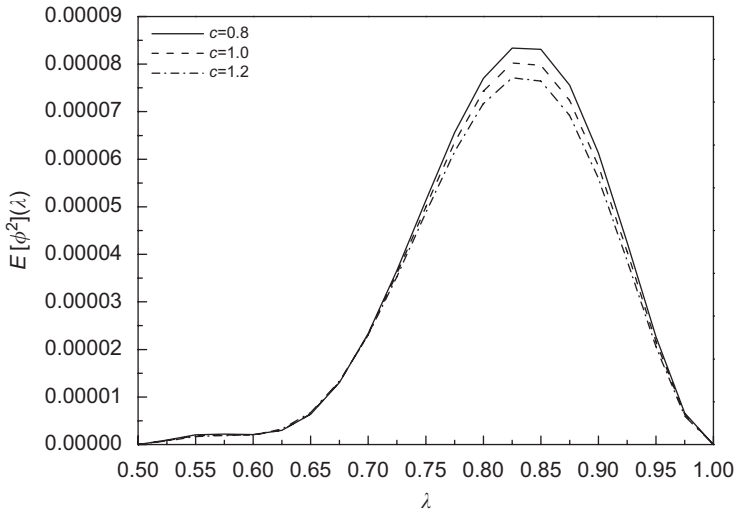

Fig. 26. Mean-square electric potential $E[\phi^2]$ versus radial coordinate λ for different structural damping coefficient c ($s_0 = 0.05$).

$H_{13}(\omega)$ and $H_{31}(\omega)$, $H_{23}(\omega)$ and $H_{32}(\omega)$ demonstrate the non-symmetry of the frequency-response function matrix $\mathbf{H}(\omega)$ or the structural system (35). Figs. 8–11 show the frequency-response functions $H_{11}(\omega)$, $H_{22}(\omega)$, $H_{33}(\omega)$, $H_{12}(\omega)$, $H_{21}(\omega)$, $H_{13}(\omega)$, $H_{31}(\omega)$, $H_{23}(\omega)$ and $H_{32}(\omega)$ of the damped piezoelectric hollow cylinder, which verify the above observation once more.

Figs. 12–19 display the mean-square radial displacement $E[u^2]$ varying with the radial coordinate λ for the piezoelectric hollow cylinder subjected to outer-boundary stochastic pressure with the power spectral density (49). The mean-square displacement $E[u^2]$ obtained by numerical simulation is given in Fig. 12, which very agrees with the result by using the proposed analysis method. Figs. 12 and 16 illustrate the mean-square displacement $E[u^2]$ increasing with the enhancement of the stochastic pressure intensity s_0 and the decrease of the pressure damping coefficient η, respectively. However, the mean-square displacement $E[u^2]$ is always close to zero at $\lambda \approx 0.75$ for different intensity s_0 and damping η. Figs. 13–15 show the mean-square displacement $E[u^2]$ varying for different dominant excitation frequency ω_0 around the 1st, 2nd and 3rd natural frequencies, respectively. It can be seen that the mean-square displacement $E[u^2]$ decreases as the domain of the dominant frequency ω_0 rises. Figs. 17 and 18 illustrate the mean-square displacement $E[u^2]$ slightly varying for different

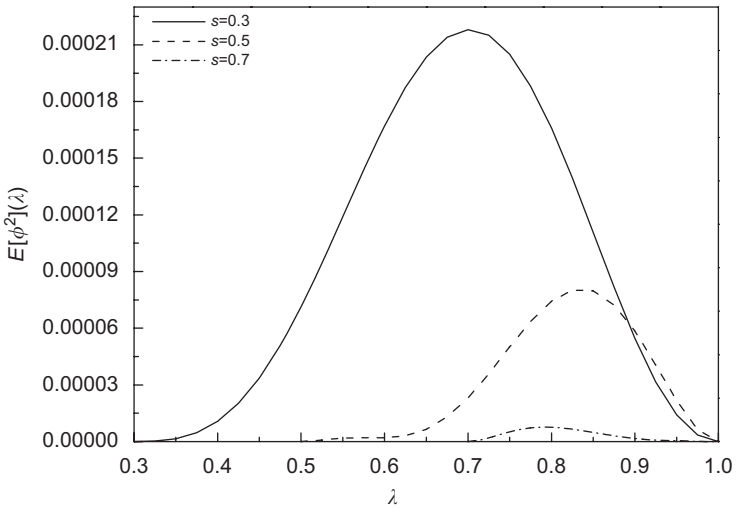

Fig. 27. Mean-square electric potential $E[\phi^2]$ versus radial coordinate λ for different ratio s of inner to outer radii ($s_0 = 0.05$).

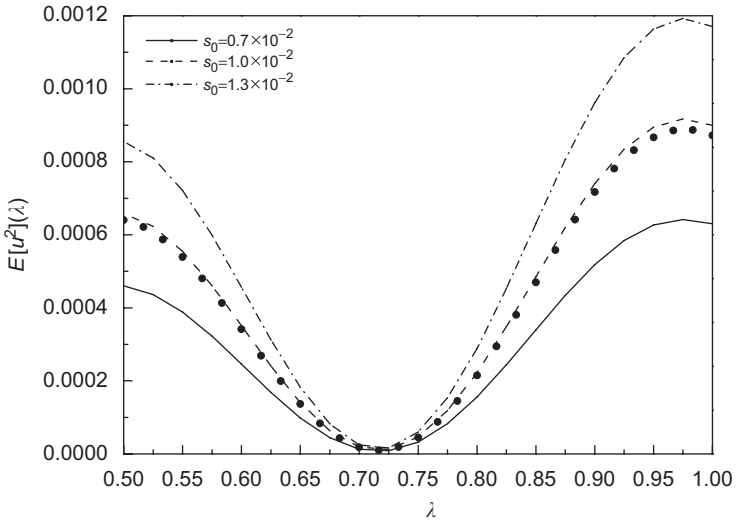

Fig. 28. Mean-square radial displacement $E[u^2]$ versus radial coordinate λ for different boundary electric-potential intensity s_0 (● by numerical simulation).

piezoelectric constant e_{33} and structural damping coefficient c, respectively. Fig. 19 shows the mean-square displacement $E[u^2]$ varying for different ratio s of inner to outer radii. It is observed again that $E[u^2] \approx 0$ at the mid-layer of the piezoelectric hollow cylinder.

Figs. 20–27 display the mean-square electric potential $E[\phi^2]$ varying with the radial coordinate λ for the piezoelectric hollow cylinder subjected to outer-boundary stochastic pressure with the power spectral density (49), or the electrical and mechanical coupling properties. The mean-square electric potential $E[\phi^2]$ obtained by numerical simulation is given in Fig. 20, which very agrees with the result by using the proposed analysis method. Figs. 20 and 24 illustrate the mean-square electric potential $E[\phi^2]$ increasing with the enhancement of the stochastic pressure intensity s_0 and the decrease of the pressure damping coefficient η, respectively. It can

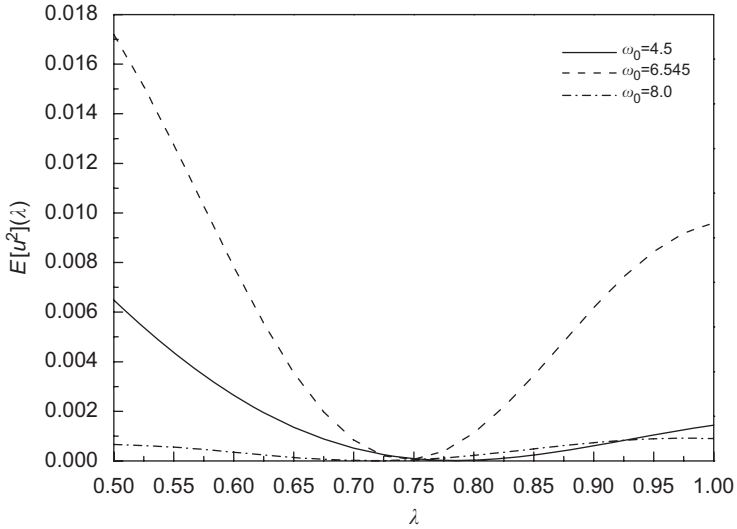

Fig. 29. Mean-square radial displacement $E[u^2]$ versus radial coordinate λ for different boundary electric-potential dominant frequency ω_0 around the 1st natural frequency ω_1 ($s_0 = 0.01$).

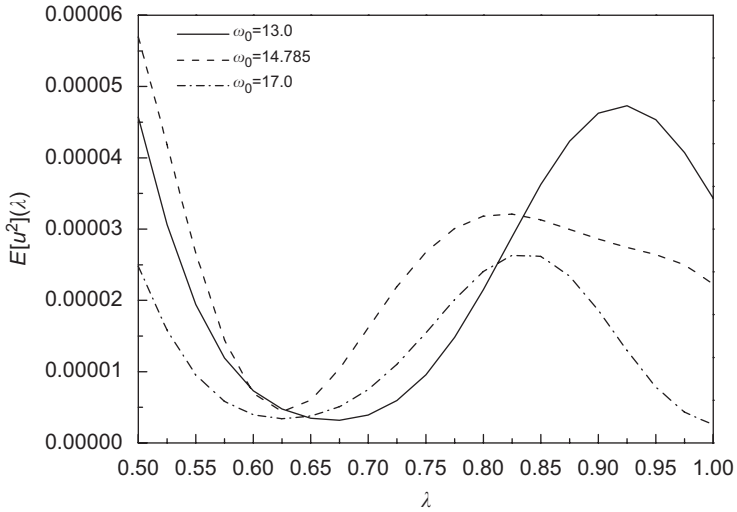

Fig. 30. Mean-square radial displacement $E[u^2]$ versus radial coordinate λ for different boundary electric-potential dominant frequency ω_0 around the 2nd natural frequency ω_2 ($s_0 = 0.01$).

be seen that the mean-square electric potential $E[\phi^2]$ approaches a maximum value at $\lambda \approx 0.85$. Figs. 21–23 show the mean-square electric potential $E[\phi^2]$ for different dominant excitation frequency ω_0. Figs. 25–27 show the mean-square electric potential $E[\phi^2]$ varying for different piezoelectric constant e_{33}, structural damping coefficient c and ratio s of inner to outer radii, respectively. The peak value of $E[\phi^2]$ is observed again and $E[\phi^2]$ increases as the thickness of the piezoelectric hollow cylinder decreases.

For the piezoelectric hollow cylinder subjected to outer-boundary stochastic electric-potential with the power spectral density (50), Figs. 28–32 illustrate the mean-square radial displacement $E[u^2]$ varying with the radial coordinate λ under various stochastic electric-potential intensities s_0, dominant excitation frequencies

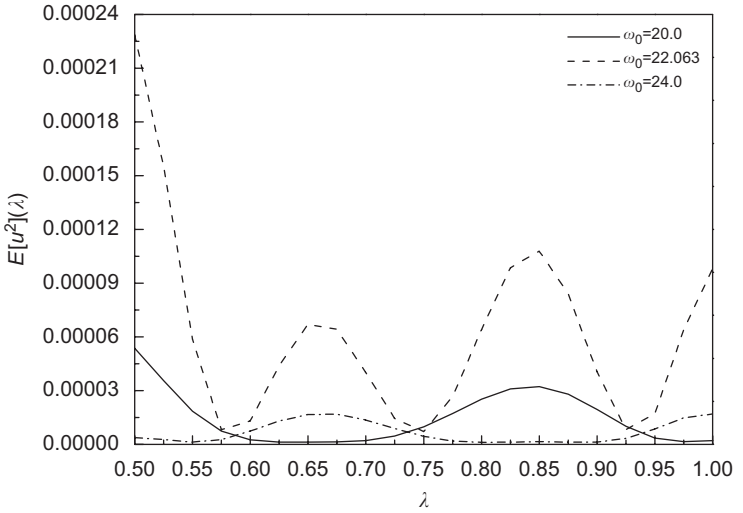

Fig. 31. Mean-square radial displacement $E[u^2]$ versus radial coordinate λ for different boundary electric-potential dominant frequency ω_0 around the 3rd natural frequency ω_3 ($s_0 = 0.01$).

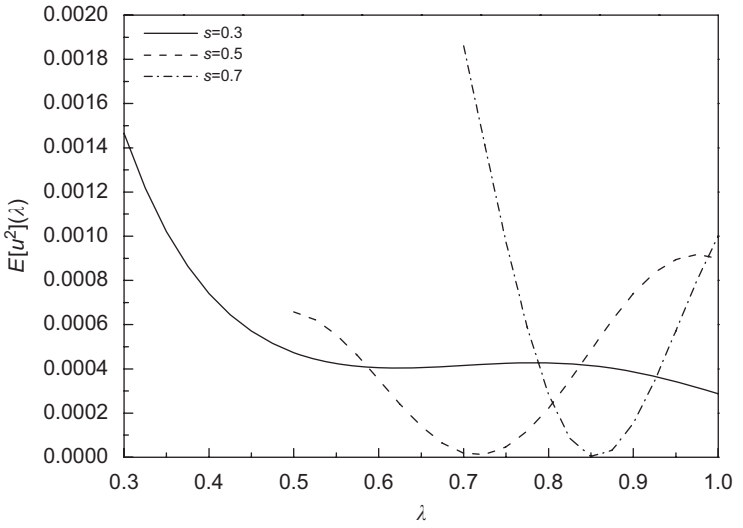

Fig. 32. Mean-square radial displacement $E[u^2]$ versus radial coordinate λ for different ratio s of inner to outer radii ($s_0 = 0.01$).

ω_0 and ratios s of inner to outer radii, respectively. It can be seen that the mean-square displacement $E[u^2]$ has a minimum value and increases with intensity s_0. The $E[u^2]$ for the dominant excitation frequency ω_0 close to the 1st structural natural frequency ω_1 is larger than that for the other ω_0. The mean-square displacement $E[u^2]$ by numerical simulation given in Fig. 28 is in good agreement with that by using the proposed analysis method.

For the piezoelectric hollow cylinder subjected to outer-boundary stochastic electric-potential with the power spectral density (50), Figs. 33–37 illustrate the mean-square electric potential $E[\phi^2]$ monotonically increasing with the radial coordinate λ under various stochastic electric-potential intensities s_0, dominant

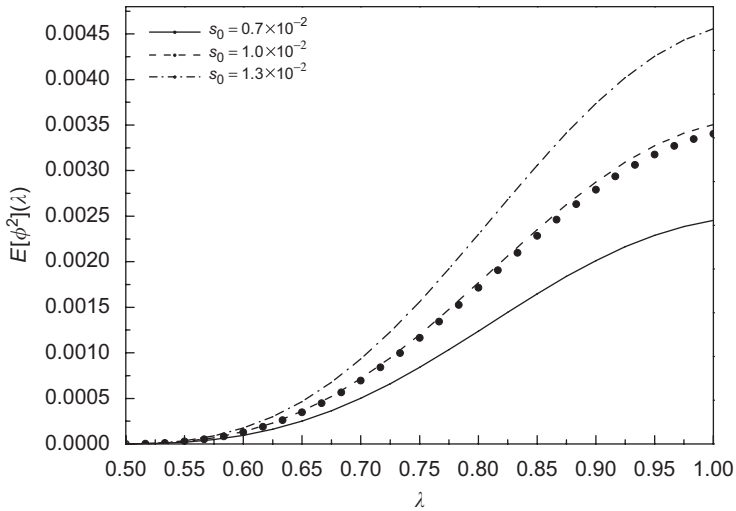

Fig. 33. Mean-square electric potential $E[\phi^2]$ versus radial coordinate λ for different boundary electric-potential intensity s_0 (● by numerical simulation).

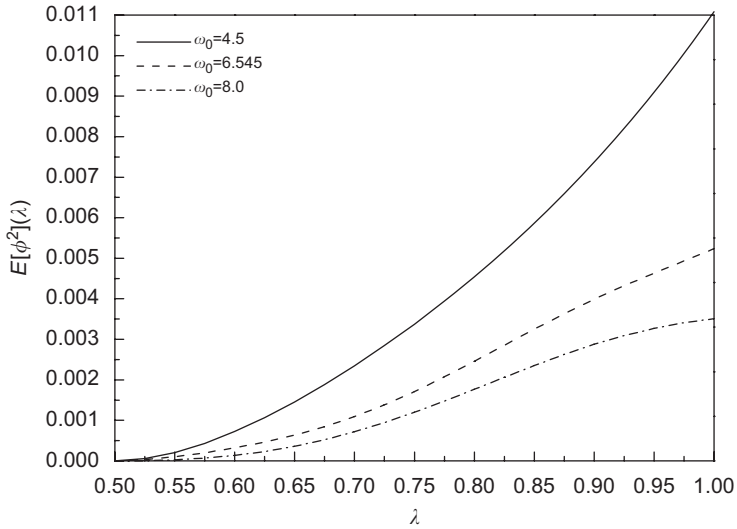

Fig. 34. Mean-square electric potential $E[\phi^2]$ versus radial coordinate λ for different boundary electric-potential dominant frequency ω_0 around the 1st natural frequency ω_1 ($s_0 = 0.01$).

excitation frequencies ω_0 and ratios s of inner to outer radii, respectively. It can be seen that the mean-square electric potential $E[\phi^2]$ increases with the enhancement of the excitation intensity s_0 and the decrease of thickness of the piezoelectric hollow cylinder. The $E[\phi^2]$ for the dominant excitation frequency ω_0 close to the 1st structural natural frequency ω_1 is larger than that for the other ω_0. The mean-square electric potential $E[\phi^2]$ by numerical simulation given in Fig. 33 is in good agreement with that by using the proposed analysis method.

7. Conclusions

A stochastic response analysis method for piezoelectric thick axisymmetric hollow cylinders subjected to boundary stochastic excitations has been proposed based on the transformations of electric potentials and

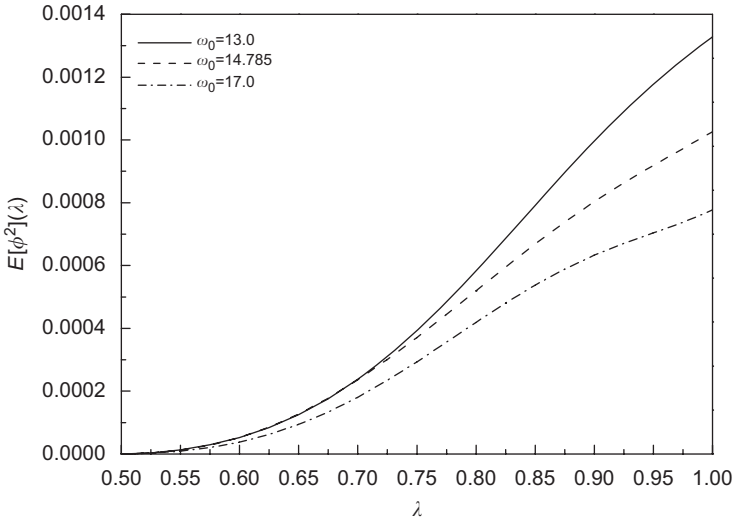

Fig. 35. Mean-square electric potential $E[\phi^2]$ versus radial coordinate λ for different boundary electric-potential dominant frequency ω_0 around the 2nd natural frequency ω_2 ($s_0 = 0.01$).

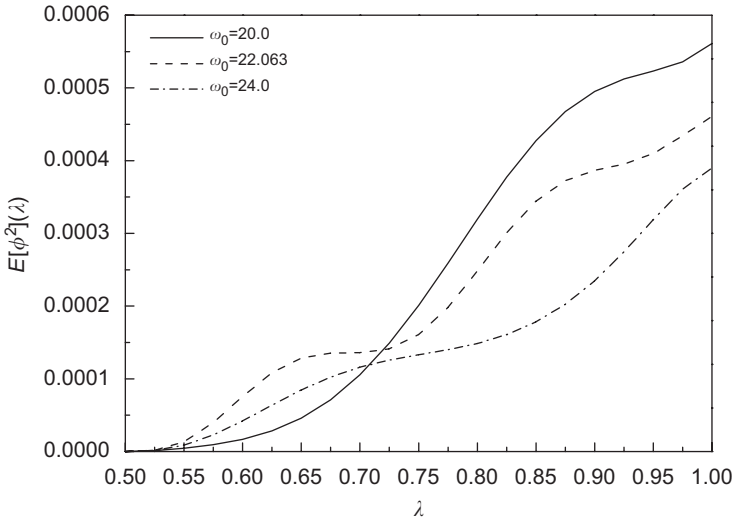

Fig. 36. Mean-square electric potential $E[\phi^2]$ versus radial coordinate λ for different boundary electric-potential dominant frequency ω_0 around the 3rd natural frequency ω_3 ($s_0 = 0.01$).

displacements, the Galerkin method and the theory of random vibration. The proposed analysis method is applicable to the hollow cylinders with arbitrary thickness under various non-white stochastic excitations of inner and/or outer pressures and electric potentials. The electrical and mechanical coupling properties and the non-symmetry of the discretized multi-degree-of-freedom system have been explored theoretically and numerically. The dynamic characteristics of the frequency-response function, mean-square displacement and mean-square electric potential have been illustrated with a great deal of numerical results on the piezoelectric hollow cylinder subjected to boundary stochastic excitations.

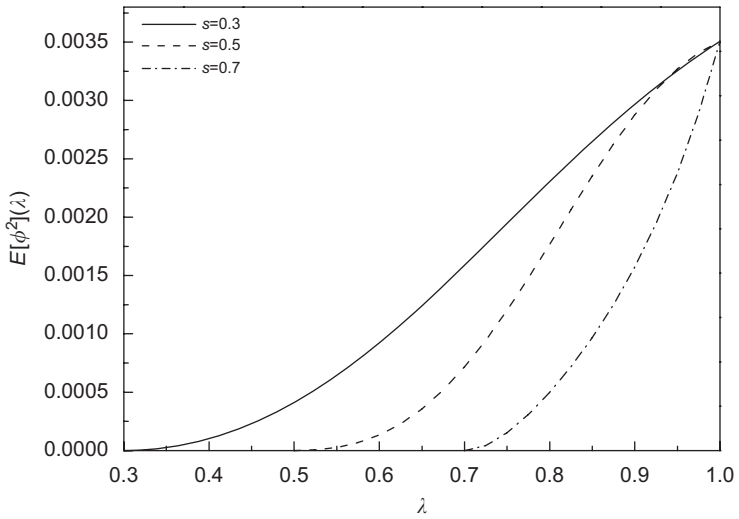

Fig. 37. Mean-square electric potential $E[\phi^2]$ versus radial coordinate λ for different ratio s of inner to outer radii ($s_0 = 0.01$).

Acknowledgment

This study was supported by the Zhejiang Provincial Natural Science Foundation of China under Grant no. Y607087.

References

[1] S.S. Rao, M. Sunar, Piezoelectricity and its use in disturbance sensing and control of flexible structures: a survey, *ASME Applied Mechanics Reviews* 47 (1994) 113–123.
[2] D.A. Saravanos, P.R. Heyliger, Mechanics and computational models for laminated piezoelectric beams, plates and shells, *ASME Applied Mechanics Reviews* 52 (1999) 305–320.
[3] H.S. Tzou, J.P. Zhong, A linear theory of piezoelastic shell vibrations, *Journal of Sound and Vibration* 175 (1994) 77–88.
[4] N.T. Adelman, Y. Stavsky, E. Segal, Axisymmetric vibration of radially polarized piezoelectric ceramic cylinders, *Journal of Sound and Vibration* 38 (1975) 245–254.
[5] H.J. Ding, R.Q. Xu, W.Q. Chen, Free vibration of transversely isotropic piezoelectric circular cylindrical panels, *International Journal of Mechanical Sciences* 44 (2002) 191–206.
[6] M. Berg, P. Hagedorn, S. Gutschmidt, On the dynamics of piezoelectric cylindrical shells, *Journal of Sound and Vibration* 274 (2004) 91–109.
[7] W.Q. Chen, H.J. Ding, R.Q. Xu, Three dimensional free vibration analysis of a fluid-filled piezoelectric hollow sphere, *Computers and Structures* 79 (2001) 653–663.
[8] P. Bisegna, G. Caruso, F. Maceri, Optimized electric networks for vibration damping of piezoactuated beams, *Journal of Sound and Vibration* 289 (2006) 908–937.
[9] K.M. Newbury, D.J. Leo, Structural dynamics of stiffened plates with piezoceramic sensors and actuators, *AIAA Journal* 39 (2001) 942–950.
[10] Q. Wang, S.T. Quek, C.T. Sun, X. Liu, Analysis of piezoelectric coupled circular plate, *Smart Materials and Structures* 10 (2001) 229–239.
[11] F. Ebrahimi, A. Rastgoo, Free vibration analysis of smart annular FGM plates integrated with piezoelectric layers, *Smart Materials and Structures* 17 (2008) 015044.
[12] M.T. Kamali, H.M. Shodja, Three-dimensional free vibration analysis of multiphase piezocomposite structures, *ASCE Journal of Engineering Mechanics* 132 (2006) 871–881.
[13] G.H. Qing, J.X. Xu, P. Li, J.J. Qiu, A new efficient numerical method and the dynamic analysis of composite laminates with piezoelectric layers, *Composite Structures* 78 (2007) 457–467.
[14] Z.C. Yang, Q.M. Wang, Transient response of piezoelectric thin-film vibration sensor under pulse excitation, *Journal of Applied Physics* 99 (2006) 014107.
[15] A. Mukherjee, A.S. Chaudhuri, Nonlinear dynamic response of piezolaminated smart beams, *Computers and Structures* 83 (2005) 1298–1304.
[16] H.J. Ding, H.M. Wang, P.F. Hou, The transient responses of piezoelectric hollow cylinders for axisymmetric plane strain problems, *International Journal of Solids and Structures* 40 (2003) 105–123.

[17] I.A. Loza, N.A. Shul'ga, Forced axisymmetric vibrations of a hollow piezoelectric sphere with an electrical method of excitation, *Soviet Applied Mechanics* 26 (1990) 818–822.
[18] H.Y. Li, Z.X. Liu, Q.R. Lin, Spherical-symmetric steady-state response of piezoelectric spherical shell under external excitation, *Applied Mathematics and Mechanics* 21 (2000) 947–956.
[19] G.R. Liu, X.Q. Peng, K.Y. Lam, J. Tani, Vibration control simulation of laminated composite plates with integrated piezoelectrics, *Journal of Sound and Vibration* 220 (1999) 827–846.
[20] H.S. Tzou, D.W. Wang, W.K. Chai, Dynamics and distributed control of conical shells laminated with full and diagonal actuators, *Journal of Sound and Vibration* 256 (2002) 65–79.
[21] S. Narayanan, V. Balamurugan, Finite element modelling of piezolaminated smart structures for active vibration control with distributed sensors and actuators, *Journal of Sound and Vibration* 262 (2003) 529–562.
[22] S.E. Miller, Y. Oshman, H. Abramovich, Selective modal control theory for piezolaminated anisotropic shells, *Journal of Guidance Control and Dynamics* 24 (2001) 844–852.
[23] S. Na, L. Librescu, Optimal vibration control of thin-walled anisotropic cantilevers exposed to blast loadings, *Journal of Guidance Control and Dynamics* 23 (2000) 491–500.
[24] L. Librescu, S. Na, Comparative study on vibration control methodologies applied to adaptive thin-walled anisotropic cantilevers, *European Journal of Mechanics A—Solids* 24 (2005) 661–675.
[25] M.S. Rao, S. Narayanan, Active control of wave propagation in multi-span beams using distributed piezoelectric actuators and sensors, *Smart Materials and Structures* 16 (2007) 2577–2594.
[26] C.W.S. To, T. Chen, Optimal control of random vibration in plate and shell structures with distributed piezoelectric components, *International Journal of Mechanical Sciences* 49 (2007) 1389–1398.
[27] R. Kumar, B. Mishra, S. Jain, Vibration control of smart composite laminated spherical shell using neural network, *Journal of Intelligent Material Systems and Structures* 19 (2008) 947–957.
[28] K.V. Sarma, Torsional wave motion of a finite inhomogeneous piezoelectric cylindrical shell, *International Journal of Engineering Science* 18 (1980) 449–454.
[29] N.A. Shul'ga, A.Y. Grigorenko, I.A. Loza, Axisymmetric electroelastic waves in a hollow piezoelectric ceramic cylinder, *Prikladnaya Mekhanika* 20 (1984) 23–28.
[30] H.S. Paul, M. Venkatesan, Vibration of a hollow circular cylinder of piezoelectric ceramics, *Journal of the Acoustical Society of America* 82 (1987) 952–956.
[31] D.A. Berlincourt, D.R. Curran, H. Jaffe, Piezoelectric and piezomagnetic materials and their function in transducers, in: W.P. Mason (Ed.), *Physical Acoustics: Principle and Methods*, 1A, Academic Press, London, 1964, pp. 63–119.